Modeling the interactions of pedestrians and cyclists in mixed flow conditions in uni- and bidirectional flows on a shared pedestrian-cycle road

Ning Guo[1], Rui Jiang[2,*], S C Wong[3,*], Qing-Yi Hao[4], Shu-Qi Xue[5], Yao Xiao[2], Chao-Yun Wu[4]

[1]*School of Automotive and Transportation Engineering, Hefei University of Technology, 230009, Hefei, P.R. China*

[2] *Key Laboratory of Transport Industry of Big Data Application Technologies for Comprehensive Transport, Ministry of Transport, Beijing Jiaotong University, 100044, Beijing, P.R. China*

[3] *Department of Civil Engineering, The University of Hong Kong Pokfulam Road, Hong Kong, P.R. China*

[4] *School of Mathematics and Computational Science, Anqing Normal University, 246133, Anqing, P.R. China*

[5] *School of Modern Posts, Xian University of Posts and Telecommunications, 710061, Xi'an, P.R. China*

Abstract

The mixed flow of pedestrians and cyclists is frequently observed on the roads they share, but investigations of the dynamics of this kind of mixed flow have been very limited. This study proposes a heuristic-based model to reproduce the mixed-flow dynamics of pedestrians and cyclists, and the model is calibrated with an experiment on the mixed traffic flow of pedestrians and cyclists. Pedestrians/cyclists were asked to walk/ride on a ring-shaped track. In the uni/bidirectional flow scenario, pedestrians and cyclists moved in the same/opposite direction. A genetic algorithm was used for parameter calibration. The model could reproduce the experimental results well. Under both scenarios, pedestrians and cyclists formed their own lanes. The pedestrians walked in the inner lane, and cyclists rode in the outer lane in a self-organized process. The widths of the pedestrian lane and the cyclist lane were found to be more uniform during bidirectional flow. The pedestrian flow rate was higher in the unidirectional flow scenario than in the bidirectional flow scenario. In contrast, at low cyclist densities, the cyclist flow rate was essentially the same in both scenarios. When the density was high, the cyclist flow rate is higher in the unidirectional flow scenario. Sensitivity analyses showed that cyclist speed had little effect on the pedestrian flow rate. A higher cyclist speed led to a higher cyclist flow rate at low densities, but the cyclist flow rates approached the same value at high cyclist densities. As the proportion of pedestrians/cyclists increased, the flow rate of cyclists/pedestrians decreased. The simulation results on a straight track were largely consistent with those on a ring-shaped track.

Keywords: Heuristic-based model, bicycle flow, pedestrian flow, lane formation

[*] Corresponding authors, Email: jiangrui@bjtu.edu.cn, hhecwsc@hku.hk.

1. Introduction

Active transport, such as walking and cycling, is an important transportation mode. As sustainable modes of transport, walking and/or cycling are often the main choices for the last mile of a trip. They not only help to reduce fuel consumption, they also alleviate traffic congestion and improve individual health. Compared to travel by car, active transport is convenient and flexible and does not pollute. Around 25% trips in the UK are by foot or cycle; this proportion is over 30% in Denmark, Finland, Germany, and Sweden and close to 50% in the Netherlands (Bassett et al., 2008), with 55% being the development goal in China (MOHURD, 2012). Thus, active transport is indispensable, and its development has effects on an area's entire road system. In-depth investigation of active transport is therefore worthwhile.

In recent years, the study of pedestrian traffic and bicycle traffic flow has attracted wide attention in the fields of physical science and engineering. Pedestrian movement is common in daily life, and complicated pedestrian behaviors can generate various self-organization phenomena (Helbing et al., 2000, 2002), such as the "fast is slow" effect, lane formation in bidirectional flow, and turbulent movement in dense crowds. Many empirical studies focus on a fundamental diagram of the relationship between speed, density, and flow (Chattaraj et al., 2009; Flötteröd and Lämmel, 2015; Navin and Wheeler, 1969; Lam et al., 2003, Helbing et al, 2005), and experiments have investigated some self-organization phenomena. Zhang et al. (2012) found that different instructions lead to different pedestrian lane configurations. Moussaïd et al. (2012) studied the phenomenon of bidirectional flow and found that traffic segregation exhibited structural instabilities characterized by the alternation of organized and disorganized states. Many models have been proposed or revised to simulate the observed characteristics, such as the continuum model (Hughes, 2002), the lattice gas model (Muramatsu et al., 1999), the floor field model (Burstedde et al., 2001), the social force model (Helbing and Molnár, 1995), and the heuristics-based model (Moussaïd et al., 2011).

The study of bicycle flow has also been explored in empirical/experimental studies and with the development of simulation models. Li et al (2015) found that overtaking is more frequent in slightly congested conditions, and that even a relatively large flow can be maintained at a relatively low average speed. An experimental study of bicycle traffic by Navin (1994) determined that the fundamental diagram predicted a maximum flow rate of 72 bic/min/m at a speed of 14 km/h and a density of 0.3 bic/m^2. Jiang et al (2017) carried out a bicycle experiment on a 146-m elliptic road with no overtaking allowed. Their data showed that when the density exceeded 0.37 bic/m, traffic jams formed spontaneously. Similar results were also reported in other experiments (Zhang et al., 2014; Zhao and Zhang, 2017). A

bicycle bottleneck flow experiment by Wierbos et al. (2019) found that the bicycle-path capacity increased with the path width and that the capacity dropped after congestion began to occur.

Models have been proposed to represent bicycle traffic flow. Jiang et al (2017) developed a cellular automaton model that was a modification of the Nagel-Schreckenberg model and it quantitatively reproduced the fundamental diagram and the occurrence of traffic jams above a critical density. Jiang et al (2004) and Jia et al (2007) proposed multivalue cellular automaton models with a stochastic randomization mechanism. Xue et al (2017) improved the multivalue cellular model by including a following move mechanism to match the experimental data and field data. Liang et al (2012) introduced psychological-physical force and trajectory choice into the model to match the speed-density relationship to the empirical data.

The mixed flow of pedestrians and cyclists can be observed on streets in the real world. Kwon et al. (1997) studied the interactions of pedestrians, bicycles, and cars in narrow urban streets in Tokyo and observed that a shorter distance between individuals resulted in higher likelihood of conflict. Zacharias (1999) found that in Amsterdam, many pedestrians and cyclists shared the street Leidsestraat. As the density on this street increased, the distance between pedestrians was observed to decrease, but the distance between cyclists and pedestrians was unchanged. Bernardi and Rupi (2015) found that the co-presence of pedestrians and cyclists in Bologna, Italy reduced the bicycle speed by 10% to 27%.

In China, the acceleration of urbanization has led to the migration of many people from rural areas to cities. This means that wider pavements and bicycle lanes are needed for the comfort and safety of both pedestrians and cyclists. However, the rapid development of motorization has resulted in the conversion of many bicycle lanes into motorized vehicle lanes. Also, many pavements serve as shared parking spaces for cars and bicycles. As a result, pedestrians and cyclists must share lanes. The mixed flow of pedestrians and cyclists is frequently observed on pedestrian-cycle-shared roads not only in urban roads but also on campus roads (Fig. 1), where walking and cycling are more popular.

Fig.1. Mixed flow of pedestrians and cyclists on the Hefei University of Technology campus. The red box indicates the measured area.

Kang et al. (2013) investigated mixed flow in Beijing, Shanghai, Hangzhou, and Hefei and observed that bicycles had a significant negative effect on pedestrian's perceptions of level of service. Xie (2009) analyzed the traffic characteristics and conflicts on pedestrian-cycle shared paths in Nanjing and provided a quality description of level of service on a shared-use path. Yu et al. (2012) found that the service level of pedestrian-cyclist mixed traffic flow improves as the road width increases and that the proportion of pedestrians significantly affects the movement of cyclists (i.e., the bicycle speed in mixed flow is 50% lower than that in pure bicycle flow). Chen and Xie (2009) developed a traffic-conflict model (overtaking conflict and avoiding conflict) for urban pedestrian-cycle roads that showed that increasing the path width helps to reduce conflict intensity between cyclists and pedestrians.

Most current studies about mixed flows of pedestrians and cyclists pay attention to the speed decrease and level of service. However, to better design pedestrian and bicycle facilities, it is important to understand the traffic dynamics of such mixed flows. Tang et al. (2010) proposed an individual-following model with a friction effect between pedestrians and cyclists and found that the friction effect would reduce cyclist flow and speed. However, this model fixed both pedestrians and cyclists in their own lanes, and collision-avoidance behavior between them was ignored. Deng (2011) set up a cellular automaton model to investigate pedestrian-cyclist mixed flow in which the pedestrian and bicycle have different geometric shapes. However, this study focused on conflict frequency, not on the interaction mechanism between pedestrians and cyclists. Mao (2015) introduced social field into the cellular automaton model to study uni- and bidirectional mixed flows on a pedestrian-cycle road. As the proportion of pedestrians increases, the traffic velocity decreases. Liu et al. (2018) built a pedestrian-movement model in pedestrian-cyclist mixed flow based on fuzzy

logic. In this model, pedestrians changed their movement intention (such as stopping, turning left/right, accelerating/decelerating) according to safety space and walking speed, but only individual movement was shown, and traffic dynamics and macroscopic characteristics were not studied.

Zacharias (1999) reported that Amsterdam authorities allowed bicycles to move on pedestrian paths because they thought pedestrians and cyclists could self-organize to avoid collisions. Unfortunately, few modeling studies of the traffic dynamics of pedestrian-cyclist mixed flows have been published, and even fewer experimental/empirical data have been used to support the reliability of the modeling of the studies that do exist. It can be inferred that three kinds of interactions occur in the complicated case: pedestrians versus pedestrians, pedestrians versus cyclists, and cyclists versus cyclists.

Motivated by this fact, we proposed and developed an improved heuristic-based model to investigate the traffic dynamics in pedestrian-cyclist mixed flow. First, we performed an experiment on mixed traffic flows including unidirectional and bidirectional flow scenarios to calibrate the model. In both simulations and experiments, the lane formation phenomenon was observed in both flow scenarios. The pedestrians/cyclists tend to form clusters when they move in the same direction. According to the fundamental diagram, the pedestrian flow rate varied less than the cyclist flow rate in the mixed traffic situation.

The paper is organized as follows: Section 2 proposes the model, Section 3 presents our experimental set-up and the results, Section 4 details the model calibration, Section 5 shows the simulation results, and conclusions are given in Section 6.

2. Model Formulation

In this section, we propose a heuristic-based model of pedestrian-cyclist mixed flow, in which both pedestrians and cyclists must choose a direction and speed for their movements. Heuristic-based models are a straightforward method for calculation of these two variables, and their description of movements is akin to that proposed by Moussaïd et al. (2011). Two heuristics based on visual information are proposed, with reference to desired moving direction and desired moving speed. The first heuristic is that a pedestrian/cyclist chooses the direction that constitutes the most direct path to their destination, taking into account the presence of obstacles. The second heuristic is that a pedestrian/cyclist maintains a distance from the first obstacle in the chosen walking/cycling direction that ensures a collision can be prevented in time. A quantitative description of these two heuristics is given in Section 2.1. Furthermore, we assume that the minimum comfortable space required by a pedestrian is formed by a circle (Fig. 2a) and that of a cyclist/bicycle is formed by three circles (Fig. 2b);

see also Guo et al. (2019). The radius of the pedestrian circle is r_p, and the radii of the cyclist circles are r_{b1}, r_{b2}, and r_{b3} for the front circle, middle circle, and rear circle, respectively.

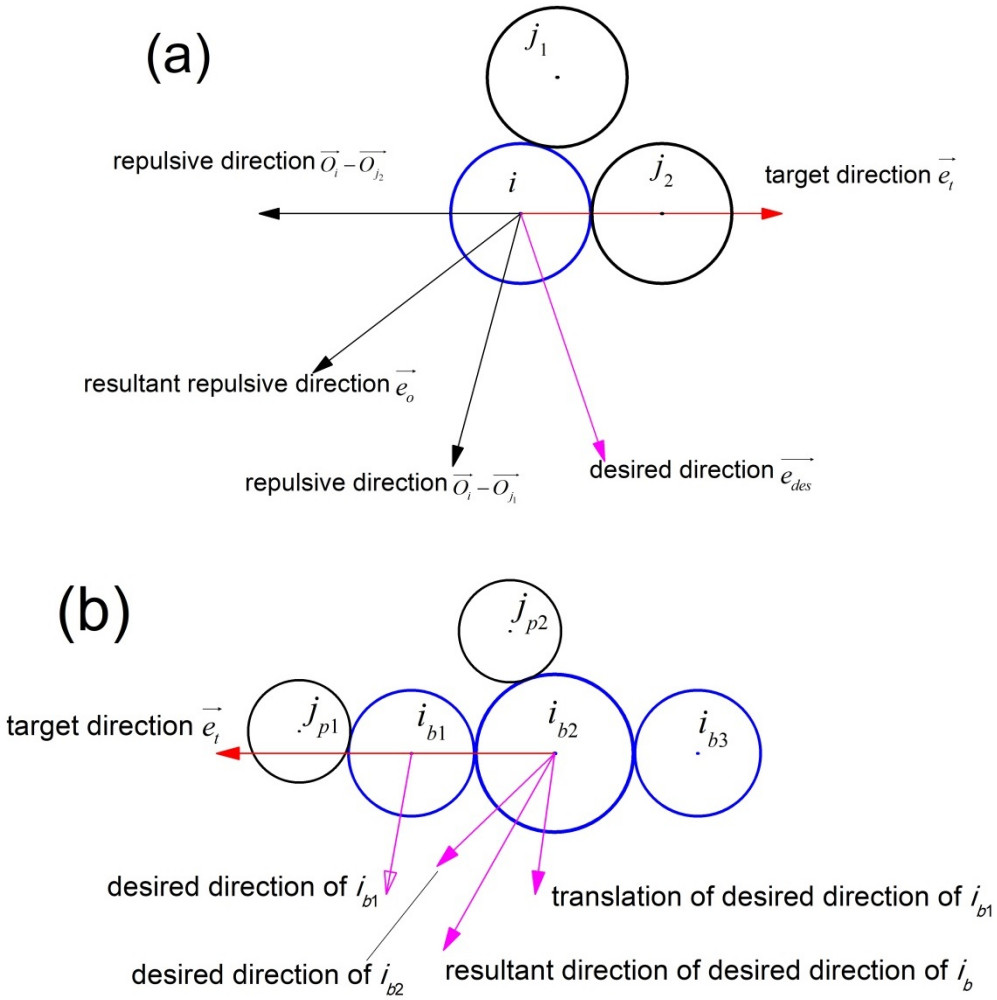

Fig. 2. Examples of desired direction. (a) Pedestrian i contacts with two circles of cyclist j_1 and j_2 moving in the opposite direction. (b) Cyclist i_b contacts with two pedestrians j_{p1} *and* j_{p2}.

We denote α_t as the angle of target movement direction, which is defined in Eq. (1) as:

$$\alpha_t = \alpha_s + \alpha_d \tag{1}$$

where α_d is angle of right/left preference. α_s is the angle of the direction along the track. We considered two kinds of tracks. For a straight track, α_s is set to be in the longitudinal direction of the track. For a ring track, α_s is set to be in the tangent direction of the track, as defined in Eq. (2):

$$\left(\cos(\alpha_s), \sin(\alpha_s)\right) = h \cdot \left(\frac{y - y_s}{D}, -\frac{x - x_s}{D} \right) \tag{2}$$

where x/x_s and y/y_s are the horizontal and vertical coordinates of the center of the

individual/track, respectively, and D is the distance between the center of the circle and the track center (Fig. 3). h is binary variable to descript the clockwise and anticlockwise movement, as in Eq.(3):

$$h = \begin{cases} 1, & clockwise \\ -1, & anticlockwise \end{cases} \tag{3}$$

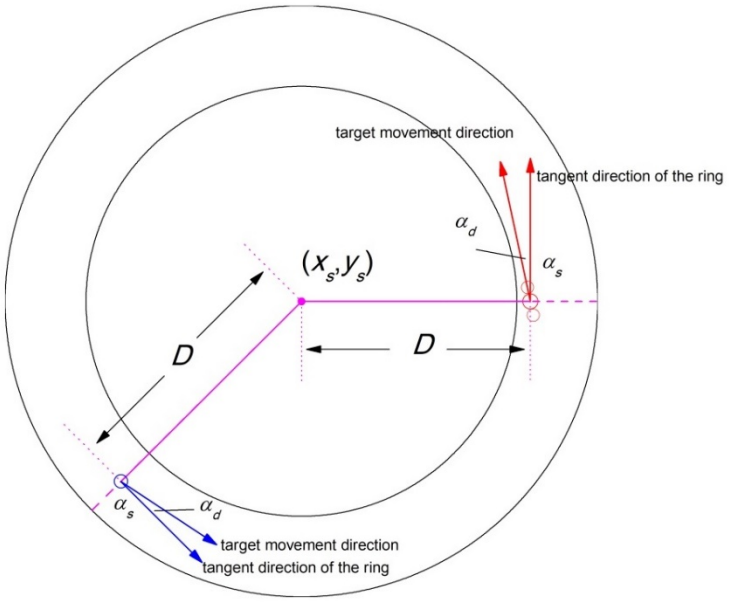

Fig. 3. Target movement direction on the ring track. Blue single circle: pedestrian; red three circles: cyclist.

2.1 Movement in the no-contact condition

In the model, it is assumed that a pedestrian/cyclist chooses his or her movement direction from the range represented by $[\alpha_t-\varphi, \alpha_t+\varphi]$. φ is the viewing range. For all candidate directions α in this range, pedestrian/cyclist i evaluates the distance to the first collision $f_1(\alpha)$, considering the other pedestrians' and cyclists' locations and speed. This model assumes that pedestrian/cyclist i wishes to move at the target speed v^{max} along the candidate direction α. In the evaluation of the first collision, it is supposed that (i), pedestrians can evaluate the current speeds of other pedestrians and cyclists accurately (as in Moussaïd et al. (2011)); (ii) cyclists can also evaluate the current speeds of pedestrians walking in the opposite direction accurately; (iii) cyclists assume that pedestrians and cyclists in the same direction do not move[1].

[1] If we change assumption (iii) and suppose cyclists assume that pedestrians and cyclists in the same direction move with current speed, then the model will significantly overestimate the flow rate, see simulation results in Appendix.

As a result, given the candidate direction α, pedestrian/cyclist i may collide with another pedestrian or cyclist after a time interval Δt. If a collision is predicted, $f_1(\alpha)$ is set to $f_1(\alpha)= v^{max}\Delta t$, denoting the distance to the first collision in direction α. If no collision will occur in direction α or $f_1(\alpha)$ exceeds a default maximum value d_{max}, then $f_1(\alpha)$ is set to $f_1(\alpha) = d_{max}$.

For potential collisions with the track boundaries, the distance $f_2(\alpha)$ is calculated by Eq (4):

$$f_2(\alpha) = \min\left[v^{max}\Delta t', d_{max}\right] \tag{4}$$

where Δt' is the time that must elapse before a collision with the boundary can occur, if a cyclist moves with speed v^{max} in direction α. If the collision distance is larger than the default maximum value d_{max}, we set it as d_{max}. Then, $f(\alpha)$ is the minimum potential collision distance in the direction α, considering other individuals and boundaries, as defined by Eq. (5):

$$f(\alpha) = \min\left[f_1(\alpha), f_2(\alpha)\right] \tag{5}$$

The chosen direction α_{des} is obtained by minimizing the function $d(\alpha)$ corresponding to the first heuristic, as per Eq. (6):

$$\alpha_{des}(t) = \arg\min\left[d(\alpha)\right] \tag{6}$$

in which $d(\alpha)$ indicates that an individual chooses the direction that allows the most direct path to the destination point while taking into account the presence of other individuals and boundaries, defined in Eq. (7):

$$d^2(\alpha) = d_{max}^2 + f^2(\alpha) - 2d_{max} f(\alpha)\cos(\alpha_t - \alpha) \tag{7}$$

where α is the variable. The desired speed $v_{des}(t)$ ensures that the individual keeps a distance from the other individuals and boundaries in the chosen movement direction that allows a time to collision of at least τ_1, given by Eq. (8):

$$v_{des}(t) = \min\left\{v^{max}, \left[f(\alpha_{des}) - vT_{safe}\right]/\tau_1\right\} \tag{8}$$

where T_{safe} denotes a safe time headway, v is the current speed, and τ_1 is the relaxation time. The calculation of the desired speed assumes that the pedestrian/cyclist may want to keep a safe distance vT_{safe} to avoid a collision, which is a new term not used by Moussaïd et al. (2011).

2.2 Movement in the contact condition

In the contact condition, the pedestrians/cyclists adjust their movement direction according to other individuals in the view, i.e., in the interval $[\alpha_t - \varphi, \alpha_t + \varphi]$. When a pedestrian's or cyclist's minimum comfortable space circle contacts the circle of a cyclist or

pedestrian traveling in the opposite direction, the pedestrian or cyclist will bypass the contacted cyclist or pedestrian. The desired direction of pedestrian/cyclist $\overrightarrow{e_{des}}$ is determined by Eq. (9):

$$\overrightarrow{e_{des}} = \frac{\vec{e_t} + \vec{e_o}}{\left|\vec{e_t} + \vec{e_o}\right|} \tag{9}$$

where the target movement direction $\vec{e_t} = [\cos(\alpha_t), \sin(\alpha_t)]$, and repulsive direction $\vec{e_o}$ is given in Eq. (10):

$$\vec{e_o} = \frac{\sum_{j \in J} \left(\vec{O_i} - \vec{O_j}\right)}{\left|\sum_{j \in J} \left(\vec{O_i} - \vec{O_j}\right)\right|} \tag{10}$$

$$\vec{O} = [x, y] \tag{11}$$

where J is the set of cyclist/pedestrian circles contacted with the pedestrian/cyclist circle i, and $\vec{O}$ is the vector form of the pedestrian/cyclist location. The desired direction is the resultant direction of the target direction and the repulsive direction (see Fig.2a).

If more than one circle of a cyclist contacts the circle of another cyclist, the desired direction is the resultant direction of the contacted multi-circles (see Fig.2b). The magnitude of the desired speed is evaluated as in Section 2.1. If a pedestrian's/cyclist's circle contacts that of other pedestrians/cyclists in the same direction, the pedestrian/cyclist behind (i.e., the pedestrian with the center of their circle behind or the cyclist with the center of their middle circle behind; in other words, the contacted ones are in the view range of the behind pedestrian/cyclist.) will stop and wait for the pedestrian/cyclist in front to move forward. If a pedestrian/cyclist's circle contacts the circles of other pedestrians/cyclists moving in both directions at the same time, the pedestrian/cyclist will stop until the pedestrians/cyclists whose circles he/she has contacted, that are in front and moving in the same direction, move away, as shown in Fig. 4.

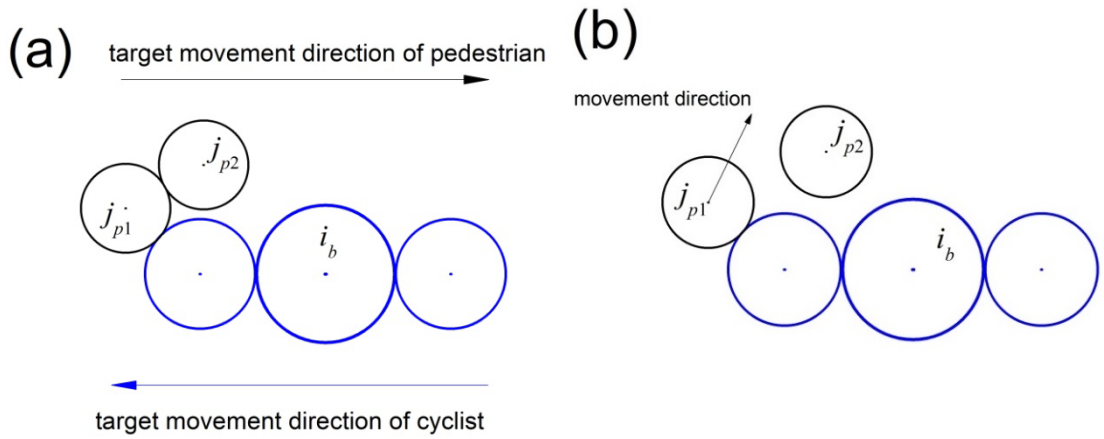

Fig. 4. Pedestrian j_{p1} contacts with the pedestrian j_{p2} and cyclist i_b in both directions. (a) Pedestrian j_{p1} stops, until (b) the front pedestrian j_{p2} moves away.

2.3 Movement acceleration

The acceleration equation used for a pedestrian is given by Eq. (12), and is the same as that in Moussaïd et al. (2011):

$$\frac{d\vec{v}}{dt} = \frac{\overrightarrow{v_{des}} - \vec{v}}{\tau_1} \tag{12}$$

As in Guo et al. (2019), it was assumed that the cyclist direction (pointing from the center of the rear circle to that of the front circle) is identical to the direction of current velocity $\vec{v}$. The vector of desired velocity $\overrightarrow{v_{des}}$ is split into two vectors, where $\overrightarrow{v_{des1}}$ along the direction of $\vec{v}$ is due to acceleration or deceleration, and $\overrightarrow{v_{des2}}$ is vertical to $\vec{v}$ and is due to the turning of the handlebars. When $\left|\overrightarrow{v_{des1}}\right| > \left|\vec{v}\right|$, the cyclist is accelerating, and when $\left|\overrightarrow{v_{des1}}\right| < \left|\vec{v}\right|$, the cyclist is decelerating. Therefore, the resulting acceleration equation is given by Eqns. (13a) and (13b):

$$\frac{d\vec{v}_i}{dt} = \begin{cases} \min\left(\left|\dfrac{\overrightarrow{v_{des1}} - \vec{v}_i}{\tau_2}\right|, a_a\right) \cdot \dfrac{\overrightarrow{v_{des1}}}{\left|\overrightarrow{v_{des1}}\right|} + \dfrac{\overrightarrow{v_{des2}}}{\tau_4}, & \left|\overrightarrow{v_{des1}}\right| \geq \left|\vec{v}_i\right| \quad (13a) \\ -\min\left(\left|\dfrac{\overrightarrow{v_{des1}} - \vec{v}_i}{\tau_3}\right|, a_d\right) \cdot \dfrac{\overrightarrow{v_{des1}}}{\left|\overrightarrow{v_{des1}}\right|} + \dfrac{\overrightarrow{v_{des2}}}{\tau_4}, & \left|\overrightarrow{v_{des1}}\right| < \left|\vec{v}_i\right| \quad (13b) \end{cases}$$

where τ_2, τ_3, τ_4 are relaxation times for acceleration, deceleration, and turning, respectively, and a_a and a_d are the maximum acceleration and maximum deceleration of the bicycle.

3 Data Collection

3.1 Experimental set-up

To calibrate the model described in Section 2, we collected data from a set of well-designed experiments performed on November 18, 2017, at Anqing Normal University in China. Experiments were conducted on an artificial ring-shaped track, such is often used to study vehicle, bicycle, and pedestrian flow (Moussaïd et al., 2012; Tadaki et al., 2013). A periodic boundary was used to maintain the density of the system. This kind of set-up removed disturbances from the density fluctuation, facilitating determination of the critical values of the phase transition. A ring-shaped track is also a common setup for implementing a periodic boundary.

The inner radius and external radius of the track were 8 m and 11 m, respectively, and the boundaries were marked with dark floor tiles and warning signs. The area of the experimental track was thus approximately 180 m^2. The participants were instructed to walk/ride on the track. A total of 160 participants (undergraduates: 47 male, 117 female) took part in the experiments, in which 80 participants were pedestrians (undergraduates: 20 male, 60 female), and the other 80 participants were cyclists (undergraduate: 27 male, 53 female). The cyclists were given a serial number from 1 to 80, and they were instructed to ride as they would in their daily life. The pedestrians were given a serial number from 101 to 180, and they were instructed to walk as they would in their daily life. In a survey after the experiment, all participants agreed that because the ring-shaped track had a large radius, they felt that the difference between riding/walking on the ring-shaped track and walking/riding on a straight track was minimal.

Six experimental runs were performed. The chronology of the experiment participant numbers is shown in Table 1. In each run, the participants were initially distributed randomly on the track. Then, the pedestrians were instructed to walk in an anti-clockwise or a clockwise direction (Table 1.), and the cyclists were instructed to ride only in an anti-clockwise direction. After three-five minutes, the participants were instructed to stop. The pedestrians were then instructed to walk in the direction opposite to that which they had been traveling previously, and the cyclists were instructed to continue riding anti-clockwise. A video camera (SONY HDR-CX510E) was used to film the experiment from a building neighboring the experimental area, and the flow rates were extracted manually from the resulting film. That is, a virtual line was drawn from the track center to its outer boundary on the film, and the number of pedestrians and cyclists passing the virtual line was counted by viewing video footage.

Table 1. Numbers of cyclist and pedestrians, serial numbers and initial directions of travel in each experimental run

Run	Number of cyclists	Serial number of cyclists	Number of pedestrians	Serial number of pedestrians	Initial direction of pedestrians
1	80	1–80	80	101–180	anti-clockwise
2	40	1–40	40	101–140	clockwise
3	70	11–80	70	111–180	anti-clockwise
4	50	1–10, 41–80	50	101–110, 141–180	clockwise
5	60	1–60	60	101–160	anti-clockwise
6	80	1–80	80	101–180	clockwise

3.2 Some observations

We now present the lane formation observed in the mixed traffic flow of pedestrians and cyclists. The most relevant factor in the lane formation phenomenon is the relative velocity difference between pedestrians and cyclists. Pedestrians and cyclists moving in clusters have more frequent interactions than when they move in lanes, until they segregate into separate lanes by moving aside whenever they encounter a different type of individual. The longest-lasting patterns of motion are those that change the least. It is obvious that such patterns correspond to lanes, as they minimize the frequency and extent of avoidance maneuvers.

In the interaction shown in Fig. 5, the converging pedestrians and cyclists move slightly to one side to avoid each other. This sideward movement tends to separate individuals moving in opposite directions. The pedestrians and cyclists separated into their own lanes soon after the beginning of the experiment. Fig. 6 shows the evolution of the average distance between pedestrians and cyclists and the track center. It can be seen that the pedestrians rapidly move to the inner boundary and the cyclists move to the outer boundary; moreover, the pedestrians always walk in the inner lane and the cyclists ride in the outer lane (see Figs. 7 and 8). This arrangement may have been due to the cyclists continuously turning throughout the experimental process, meaning that if they moved close to the inner boundary to avoid pedestrians, they would have had to increase their angle of turning. This would have been a less comfortable operation than the reduced angle of turning required when they rode closer to the outer boundary. In contrast, the pedestrians had more flexibility of movement, and could thus cope more easily with the increased turning angle required when traveling on the inner lane. Moreover, pedestrians and cyclists moving in uniform lanes will have very

rare and weak interactions. Hence, the tendency to break up existing lanes is negligible when the fluctuations are small. Furthermore, the most stable configuration corresponds to a state with a minimal interaction rate and is related to a maximum efficiency of motion.

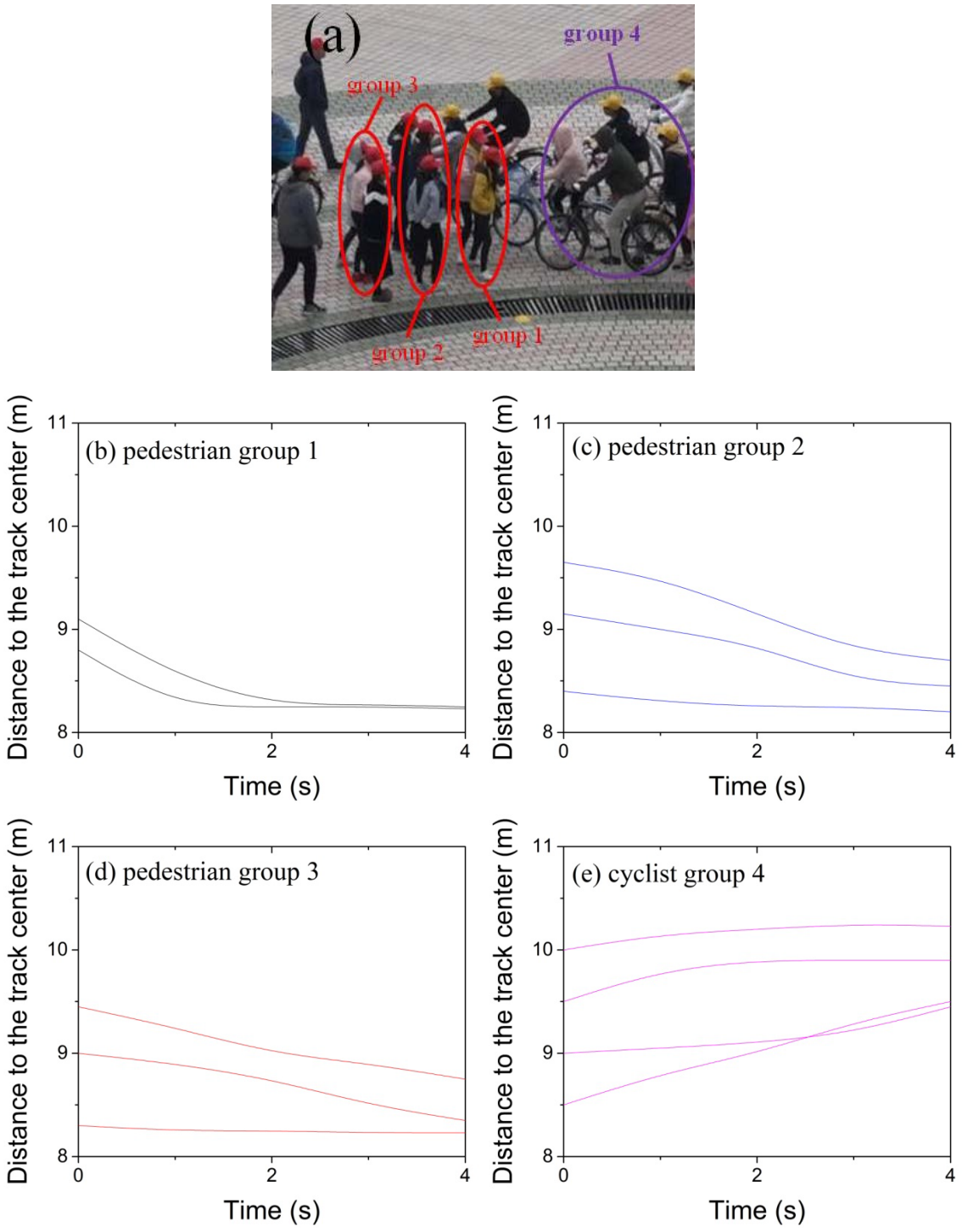

Fig. 5 A local interaction between pedestrians and cyclists in bidirectional flow. (a) Snapshot. Evolution of polar radius of (b) pedestrians in group 1, (c) pedestrians in group 2, (d) pedestrians in group 3, (c) cyclists in group 4.

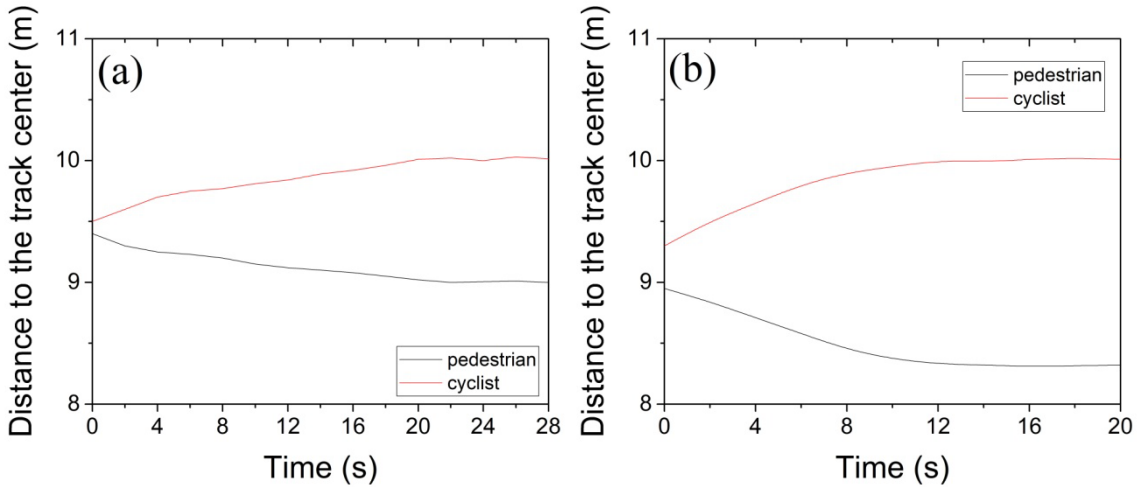

Fig.6. Evolution of average distance between pedestrian/cyclist and track center in (a) 80 pedestrians + 80 cyclists experiment in unidirectional flow; (b) 50 pedestrians + 50 cyclists experiment in bidirectional flow.

Fig. 7. Snapshots of 80 pedestrians + 80 cyclists experiment. (a) Unidirectional flow, (b) bidirectional flow.

Fig. 8. Snapshots of 40 pedestrians + 40 cyclists experiment. (a) Unidirectional flow, (b) bidirectional flow.

In the unidirectional flow scenario, it was frequently observed that three or more pedestrians walked side-by-side; this can be seen in the red box in Figs. 7(a) and Fig.8(a). One can also observe that the cyclists sometimes occupied nearly the whole width of the track, as seen in the yellow box in Figs. 7(a) and 8(a). As a result, the width of the pedestrian/cyclist lane was not uniform. In contrast, in the bidirectional flow scenario, both

the pedestrians and the cyclists actively avoided each other. Pedestrians were noted to usually walk individually, or two pedestrians were seen to walk side-by-side, as illustrated in Figs. 7(b) and 8(b). Three or more pedestrians were seldom observed to walk side-by-side. In general, the widths of both cyclist lanes and pedestrian lanes were largely uniform during bidirectional flow (Fig. 9). When the velocity difference is greater, more serious delays and potential energy costs will occur in the interaction between pedestrians and cyclists. Therefore, to minimize the conflict disturbance, pedestrians and cyclists in a bidirectional flow segregate into lanes more thoroughly than those in a unidirectional flow. As shown in Fig. 10, there is little overlap between pedestrians and cyclists in the polar direction in the bidirectional flow.

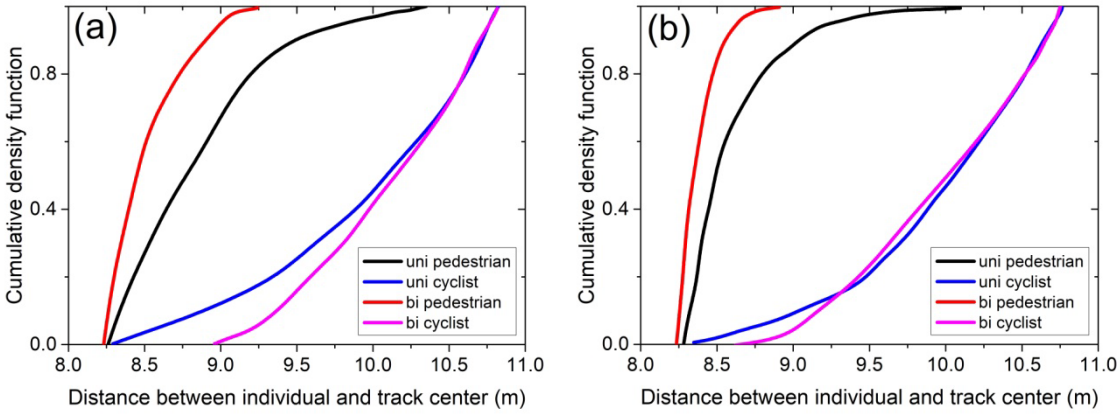

Fig. 9. Cumulative density function of distance between pedestrians/cyclists and track center in the whole experiment process. (a) 80 pedestrians + 80 cyclists (b) 40 pedestrians + 40 cyclists.

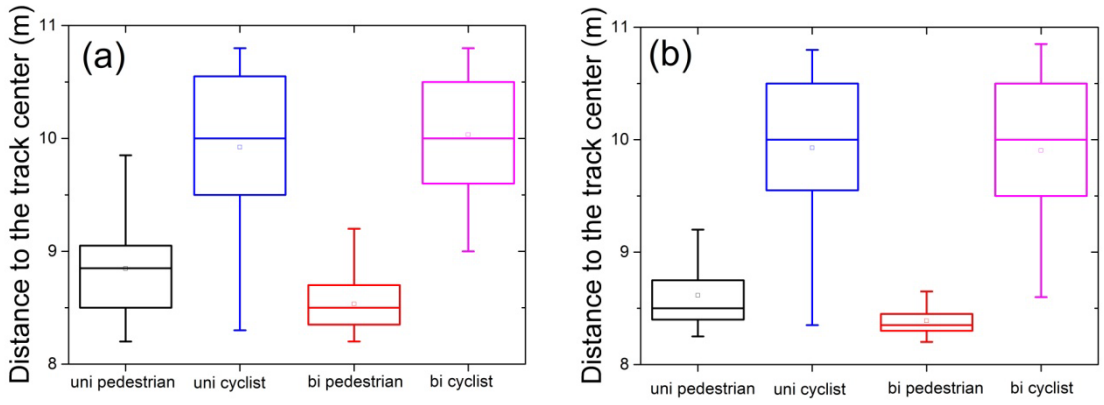

Fig. 10. Boxplot of distance between pedestrian/cyclist and track center. (a) 80 pedestrians+80 cyclists (b) 40 pedestrians+40 cyclists.

Next, we studied the fundamental diagram of the flow rate versus the global density to

examine the effect of pedestrian/cyclist numbers on the system performance. The global density of pedestrians is given by Eq. (14):

$$\rho_p = \frac{N_p}{S} \tag{14}$$

where N_p is the number of pedestrians, and S is the area of the track.

The flow rate q_p is defined as the number of pedestrians crossing a line segment perpendicular to their movement direction per unit time and per unit width, as expressed in Eq. (15):

$$q_p = \frac{N_{p,c}}{(T - T_c) \cdot w} \tag{15}$$

where w is the width of the track, and equal to 3 m, T equals the duration of experiment, T_c = 30 s (the transient time at the beginning of each experiment that is excluded), and $N_{p,c}$ is the number of pedestrians crossing a line segment from T_c to T. We confirmed that the flow rate at different widths was almost equal.

Similarly, the global density of cyclists is given by Eq. (16):

$$\rho_b = \frac{N_b}{S} \tag{16}$$

where N_b is the number of cyclists. And the cyclist flow rate q_b is given by Eq. (17):

$$q_b = \frac{N_{b,c}}{(T - T_c) \cdot w} \tag{17}$$

where $N_{b,c}$ is the number of cyclists crossing a line segment from T_c to T.

In Fig. 11 the pedestrian/cyclist flow rates during unidirectional flow are compared with those during bidirectional flow. Fig. 11a shows that in both scenarios the maximum pedestrian flow rate was reached at $\rho \approx 0.389$ pedestrians/m^2. Moreover, the pedestrian flow rate in unidirectional flow was always larger than that in bidirectional flow because in the bidirectional flow scenario, the pedestrians could see the oncoming bicycles and therefore attempted to avoid them. This collision-avoidance behavior limited the pedestrians' walking speed. However, in unidirectional flow the pedestrians could not see the bicycles because they were approaching from behind, and they thus walked less conservatively. In contrast, Fig. 11(b) shows that the cyclist flow rates at low densities were essentially the same under the two scenarios, whereas at high densities, the cyclist flow rate in the unidirectional scenario was a little larger.

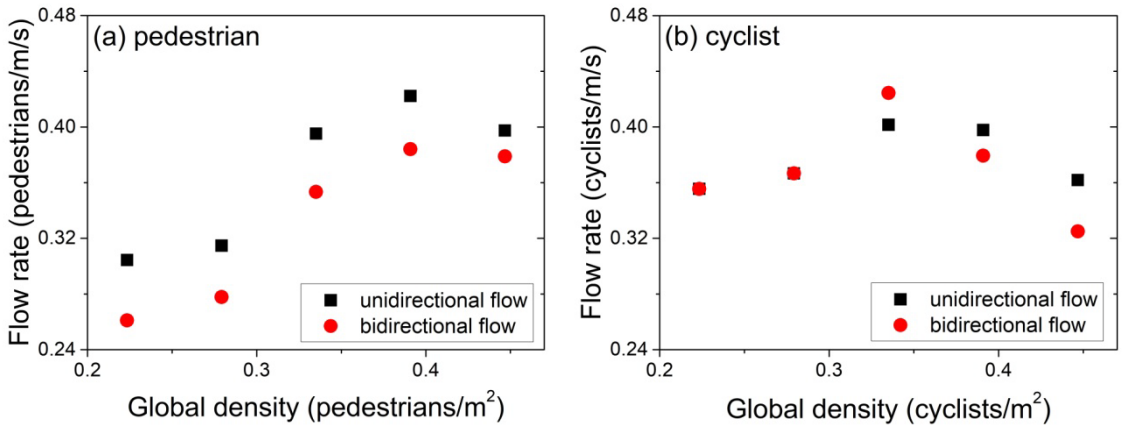

Fig. 11. Comparison between unidirectional flow and bidirectional flow. (a) Pedestrian flow, (b) cyclist flow in mixed flow. The results of the 80 pedestrians + 80 cyclists experiment are averaged over two runs.

Fig. 12(a) depicts the flow rate of pedestrians and cyclists in unidirectional flow. As the flow density increased, the flow rate of cyclists varied less than that of pedestrians. The pedestrian flow rate was lower than cyclist flow rate at low densities, but higher at high densities. Fig. 12(b) depicts the pedestrian/cyclist flow rate in bidirectional flow. The trend here was similar to that observed in unidirectional flow, with the cyclist flow rate being greater at low densities and lower at high densities.

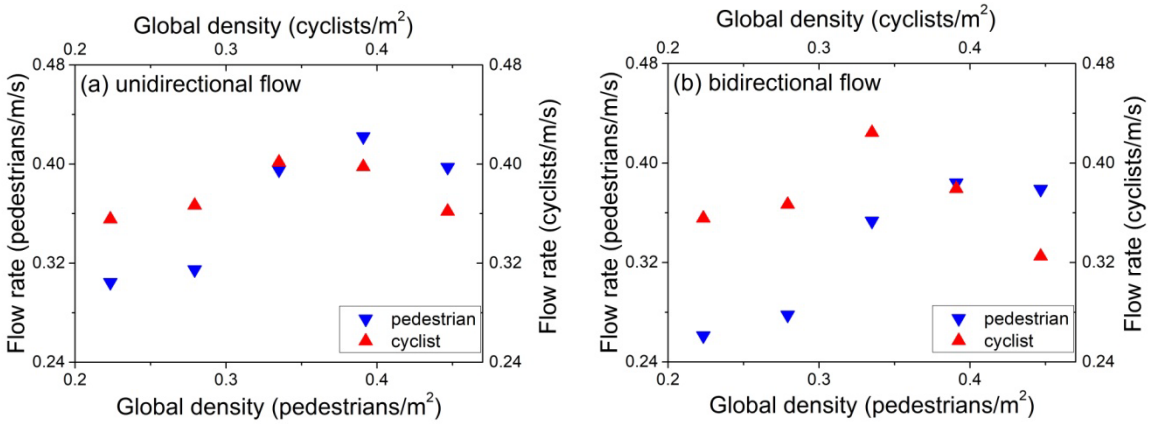

Fig. 12. Fundamental diagram of mixed flow of pedestrians and cyclists. (a) Unidirectional flow, (b) bidirectional flow. The results of 80 pedestrians + 80 cyclists experiment are averaged over two runs.

4. Model Calibration

We used the calibration method of Davidich and Köster (2012). The individual fitness is defined in Eq. (18) as:

$$F = 1 \Big/ \sum_{m}^{5} \left(\left| flow_m^{exp.p} - flow_m^{sim.p} \right| + \left| flow_m^{exp.b} - flow_m^{sim.b} \right| \right) \tag{18}$$

where $flow_m^{exp.p}$ / $flow_m^{exp.b}$ is the average flow rate of pedestrians/cyclists in the experiment, $flow_m^{sim.p}$ / $flow_m^{sim.b}$ is the simulated flow rate of pedestrians/cyclists at the same density, m = 1–5 and corresponds to the five different global densities. A genetic algorithm was used for parameter calibration. The probability of selecting an individual is given by Eq. (19):

$$P_l = F_l \Big/ \sum_{n} F_l \tag{19}$$

where F_l is the fitness value of individual l, and n is the number of individuals. The crossover rate was 0.6, and the mutation rate was 0.05. The optimization process was repeated 10 times, and the best set of values was selected. In the simulation, the size of the three-circle shape matched the size of a real bicycle, and the pedestrian radius was set to 0.2 m. The radii of the three cyclist circles were set as r_{b1} = 0.225 m, r_{b2} = 0.25 m, r_{b3} = 0.225 m, as these sum to 0.7 m, which is half the length of a bicycle. Based on physiological features related to safety engineering (He and Lin, 2000), the viewing range φ was set to 90°, and $d_{\max}$ was set to 5 m. According to the mechanical characteristics of bicycles, the maximum acceleration a_a was set to 3 m/s^2, and the maximum deceleration a_d was set to 6 m/s^2. Fig. 13 shows the convergence process of the parameter calibration, and the calibrated values are listed in Table 2 and Table 3. The maximum speed of cyclists 2 m/s is rather low, and was due to its being cold and windy on the day of the experiment. Therefore, participants rode slowly.

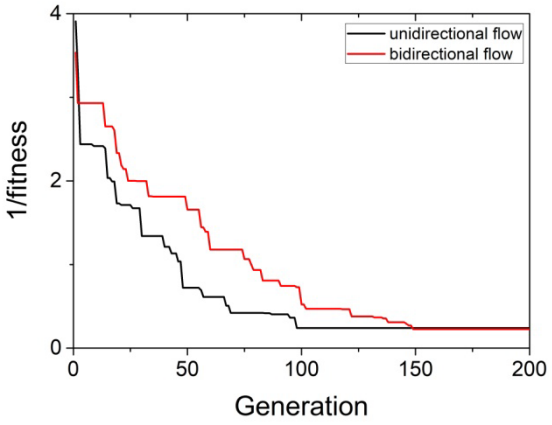

Fig. 13. Convergence plot of the genetic algorithm calibration process.

Table 2. Calibrated parameter values for pedestrians.

Parameter	Unidirectional flow	Bidirectional flow
α_d (°)	8	-10
$v_{\max}$ (m/s)	1.3	
τ_1 (s)	0.5	
T_{safe} (s)	0.25	

Table 3. Calibrated parameter values for cyclists.

Parameter	Unidirectional flow	Bidirectional flow
α_d (°)	4	2
v_{max} (m/s)	2	
τ_1 (s)	0.75	
τ_2 (s)	0.5	
τ_3 (s)	0.1	
τ_4 (s)	0.1	
T_{safe} (s)	0.15	

5. Simulation Results

5.1 Comparison with experimental data

We compared the simulated and experimental results for the pedestrian/cyclist distribution. Figs. 14 and 15 show typical simulation results for experiments comprising 80 pedestrians + 80 cyclists, and experiments comprising 40 pedestrians + 40 cyclists. The pedestrians and cyclists again segregated into lanes soon after the simulation began, as shown by the evolution of average distance between pedestrians/cyclists and the track center in Fig. 16. The pedestrians always walked along the inside boundary, and the widths of the lanes during bidirectional flow were more uniform than those in unidirectional flow; in the latter, the pedestrians and cyclists tended to aggregate in clusters, as indicated by the magenta box in Figs. 14(a) and 15(a).

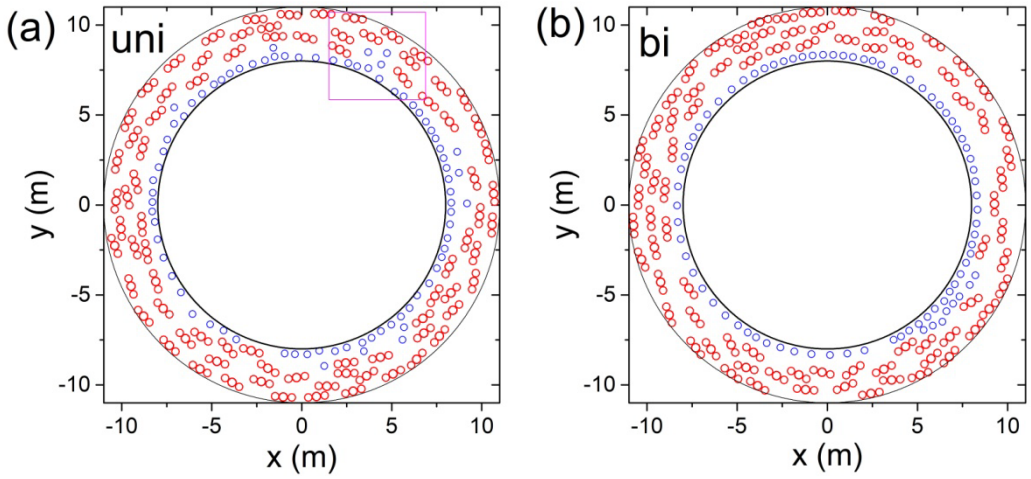

Fig. 14. Snapshots of simulations of 80 pedestrians + 80 cyclists experiment. (a) Unidirectional flow, (b) bidirectional flow. Blue single circle: pedestrian; red three circles:

cyclist.

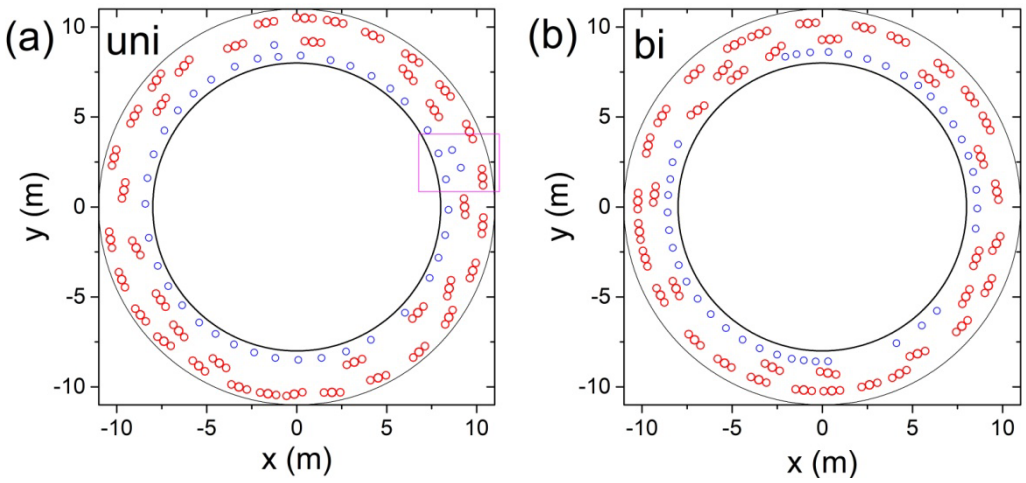

Fig. 15. Snapshots of simulations of 40 pedestrians + 40 cyclists experiment. (a) Unidirectional flow, (b) bidirectional flow. Blue single circle: pedestrian; red three circles: cyclist.

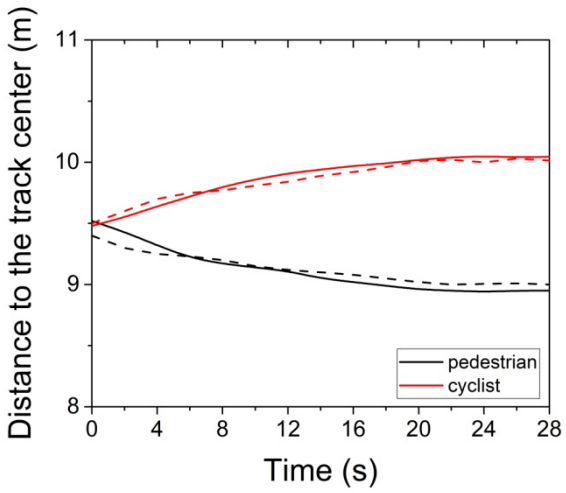

Fig.16. Evolution of average distance between pedestrian/cyclist and track center in 80 pedestrians + 80 cyclists simulation in unidirectional flow. Dashed line: experimental result; solid line: simulation result.

Fig. 17 shows the cumulative density function of the distance between the pedestrians/cyclists and the track center in these simulations. The pedestrians and cyclists were distributed in narrower polar radius intervals in bidirectional flow than they were in unidirectional flow. Finally, Figs. 18 and 19 depict the relationship between density and flow rate. One can see that the simulation results were largely in agreement with the experimental results. Table 4 shows the RMSEs and p values of paired t-tests of simulated and experimental flow rate. All RMSEs are less than 0.03 and p values are larger than 0.05,

indicating that the simulated and experimental flow rates were not significantly different.

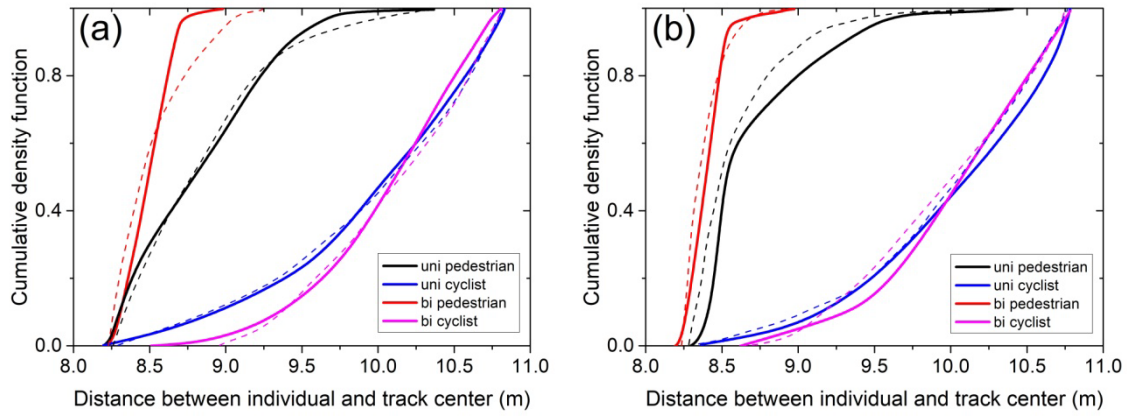

Fig. 17. Cumulative density function of distance between pedestrians/cyclists and track center in simulations. (a) 80 pedestrians + 80 cyclists (b) 40 pedestrians + 40 cyclists. Dashed line: experimental result; solid line: simulation result.

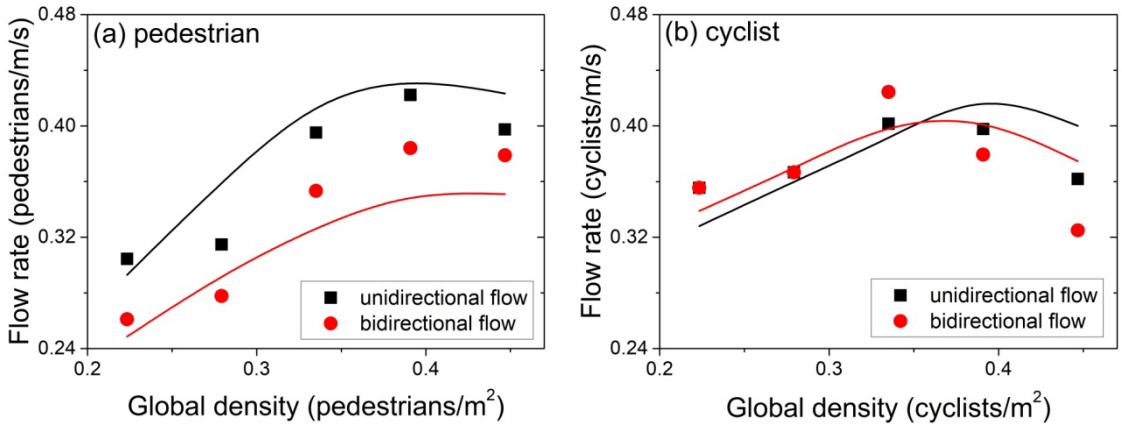

Fig. 18. Comparison of unidirectional flow and bidirectional flow in simulations. (a) pedestrian flow, (b) cyclist flow in the mixed flow. Symbol: experimental result; line: simulation result.

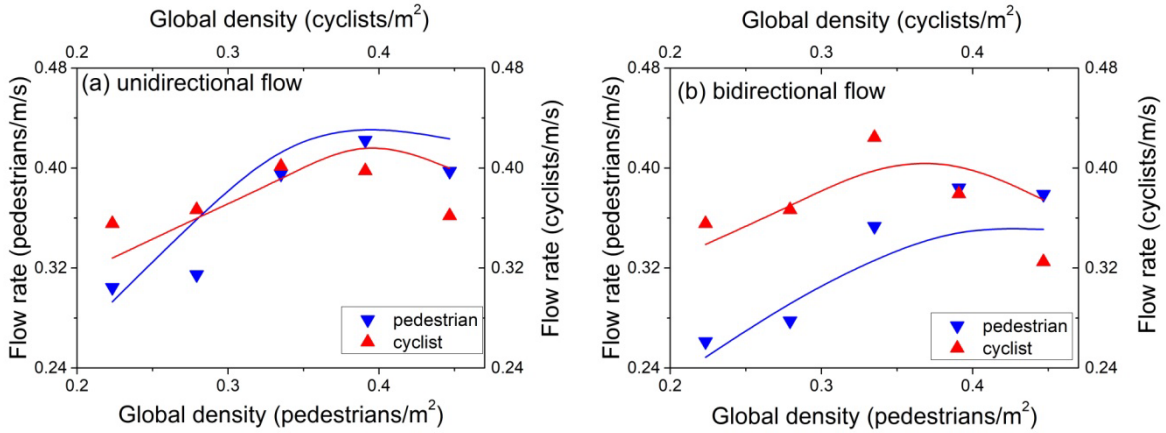

Fig. 19. Fundamental diagram of mixed flow of pedestrians and cyclists in simulations. (a) Unidirectional flow, (b) bidirectional flow. Symbol: experimental result; line: simulation result.

Table 4. RMSE and *p* value of paired *t*-test between simulated and experimental flow rate.

	Unidirectional flow		Bidirectional flow	
	Pedestrian	cyclist	Pedestrian	cyclist
RMSE	0.020	0.028	0.024	0.028
p	0.114	0.846	0.127	0.570

Some quantitative differences between the simulated and experimental results can be observed. In Fig. 18(a), the simulated flow rates in both the unidirectional and bidirectional scenarios are larger than the experimental flow rates in the experiment comprising 50 pedestrians + 50 cyclists. At high densities, the simulated flow rates in the unidirectional/bidirectional scenarios were a little larger or smaller than the corresponding experimental values. Fig. 18(b) shows that the simulated critical densities of peak cyclist flow rate in both the unidirectional and bidirectional scenarios were larger than the experimental values. The peak flow rate in the unidirectional/bidirectional scenario was also a little larger/smaller than the experimental peak-flow rate. These differences between experiment and simulation may be due to three reasons: (1) Aside from the 80 pedestrians + 80 cyclists case, all experiments were conducted only once, and thus the experimental data may not be so accurate representative of the real situation. (2) The model needs further improvement; e.g., factors such as heterogeneity and stochasticity need to be considered. (3) The model does not consider the group behavior of the pedestrians and cyclists. We compare the experimental and simulation results for the average distance between 80 pedestrians, 80 cyclists, and the track center in a bidirectional flow in the stable state. The radius of the pedestrian lane is around 8.53/8.32 m in the experiment/simulation, respectively, and the radius of the bicycle lane is

around 10.08/9.85 m in the experiment/simulation, respectively.

5.2 Validation by empirical data

We collect the mixed flow data on a straight track in the university campus, as shown in Fig. 1. The measured area is 8 m long and 3.9 m wide. The density and flow rate are measured. The pedestrian density in the time interval [t_1, t_2] is measured by Eq. (20), as proposed in Zhang et al. (2011),

$$\rho_l^p = \frac{1}{t_2 - t_1}\int_{t_1}^{t_2} \frac{N_l^p(t)}{s_l} dt \tag{20}$$

$N_l^p(t)$ is the number of pedestrians in the measured area at time t and s_l is the size of the measured area. Similarly, the cyclist density is measured by Eq. (21),

$$\rho_l^b = \frac{1}{t_2 - t_1}\int_{t_1}^{t_2} \frac{N_l^b(t)}{s_l} dt \tag{21}$$

$N_l^b(t)$ is the number of cyclists in the measured area at time t.

The flow rate is calculated by counting the number of cyclists and pedestrians passing the center line of the area during the time interval [t_1, t_2] per unit of time and per unit of walkway width.

In the simulation, the parameter values are the same as in Table 2 and Table 3, except that, α_d is set to 0 and v_{max} of the cyclist is set to 3.5 m/s, as measured in the field. We compare the empirical data and simulated results in Table 5. The simulation results are in agreement with the empirical results.

Table 5. Comparison between empirical and simulated results for a unidirectional flow on the straight track.

Density		Empirical flow rate		Simulated flow rate	
pedestrians/m^2	cyclists/m^2	pedestrians/m/s	cyclists/m/s	pedestrians/m/s	cyclists/m/s
0.096	0.032	0.140	0.128	0.146	0.126
0.224	0.032	0.313	0.079	0.322	0.077
0.288	0.032	0.461	0.064	0.455	0.063
0.385	0.032	0.513	0.051	0.519	0.052
0.417	0.032	0.556	0.064	0.561	0.063
0.064	0.064	0.093	0.205	0.090	0.204
0.449	0.096	0.552	0.103	0.556	0.104
0.577	0.096	0.659	0.070	0.653	0.072

5.3 Sensitivity analyses

We perform a sensitivity analysis of the model parameters. First, it is found that the variation in the parameter value of pedestrians/cyclists only moderately affects the flow rate of pedestrians/cyclists, because pedestrians and cyclists are separated after lane formation. Moreover, the trend of the bidirectional flow is qualitatively similar to that of the unidirectional flow. Therefore, we only present the results for the unidirectional flow.

The flow rates of pedestrians/cyclists at low densities are almost independent of τ_1 or T_{safe} (see Fig. 20 and Fig. 21(a) and (b)), because pedestrians/cyclists have enough space to maintain a high speed, even if they prefer a large collision relaxation time or safe time headway. At high densities, a smaller τ_1 or T_{safe} leads to higher pedestrian/cyclist flow rates, because in the condition with insufficient space, pedestrians/cyclists have to decrease their speed if they prefer a large collision relaxation time or safe time headway.

We can expect the acceleration time τ_2 and deceleration time τ_3 to have opposite impacts. As expected, τ_2 has a similar impact to τ_1 on the fundamental diagram, and τ_3 has the opposite impact on the flow rate (see Fig. 21(c) and (d)). Finally, τ_4 has a trivial effect on the flow rate (Fig. 21(e)).

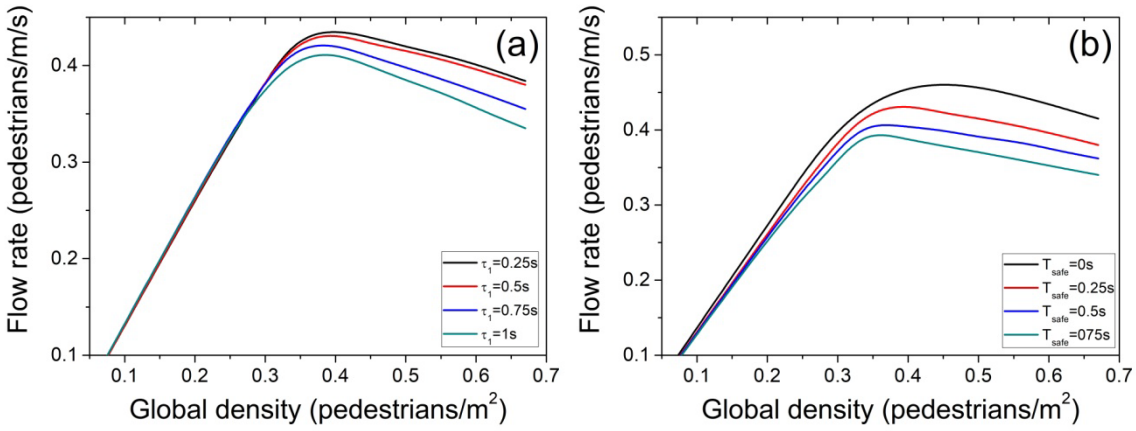

Fig. 20. Flow rate versus density of the unidirectional flow on a ring-shaped track at different (a) τ_1, (b) T_{safe} for pedestrians.

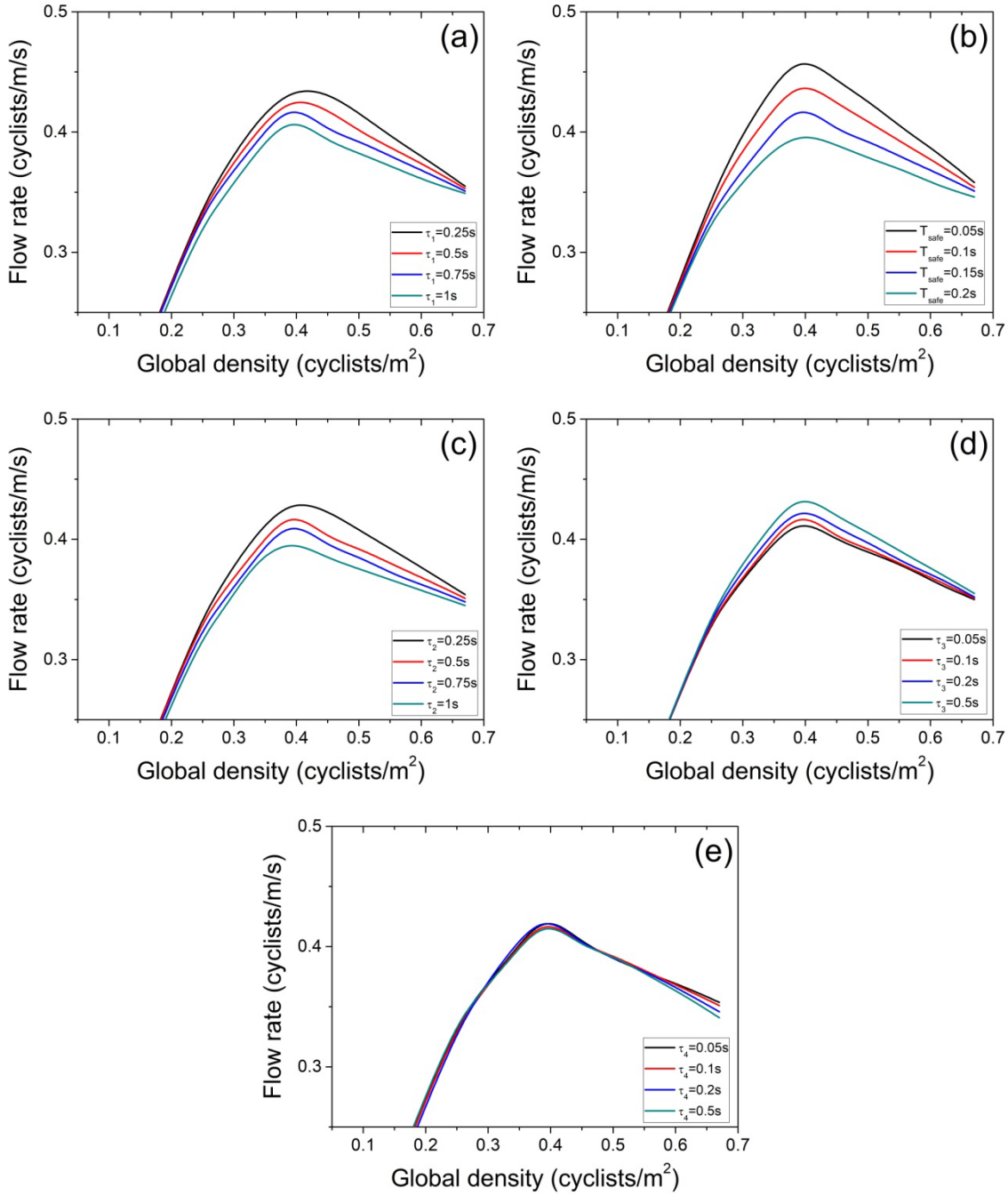

Fig. 21. Flow rate versus density of the unidirectional flow on a ring-shaped track at different (a) τ_1, (b) T_{safe}, (c) τ_2, (d) τ_3, (e) τ_4 for cyclists.

Electric bicycles powered by both electric motors and pedaling have a higher maximum speed than traditional pedal bicycles, which are powered only by the rider. Fig. 22 shows the relationship between flow rate and density at different maximum bicycle speeds. Fig. 22(a) and Fig. 22(c) show that greater maximum bicycle speeds had little effect on the unidirectional or bidirectional flow rate of pedestrians; rather, as pedestrians and cyclists segregated into lanes, pedestrian density was the key factor influencing pedestrian flow rate.

With increasing pedestrian density, the flow rate initially increased, in both the unidirectional and bidirectional scenarios; then, after reaching the critical density, the flow rate decreased. The critical density in the unidirectional scenario was less than that in the bidirectional scenario, but the flow rate was a little greater in the unidirectional scenario. However, Fig. 22(b) and Fig. 22(d) show that at low densities, a greater maximum velocity for bicycles gave rise to greater cyclist flow rates, and that as the density of cyclists increased, the flow rates at high densities were very similar. At low densities, there was enough free space for cyclists to maintain a relatively greater speed, and cyclists' interactions with pedestrians or other cyclists were infrequent. Thus, lower maximum speeds led to lower flow rates. As the density increased, there was not enough free space for cyclists to maintain a high speed; thus, cyclists' and pedestrians' flow rates were similar at higher densities.

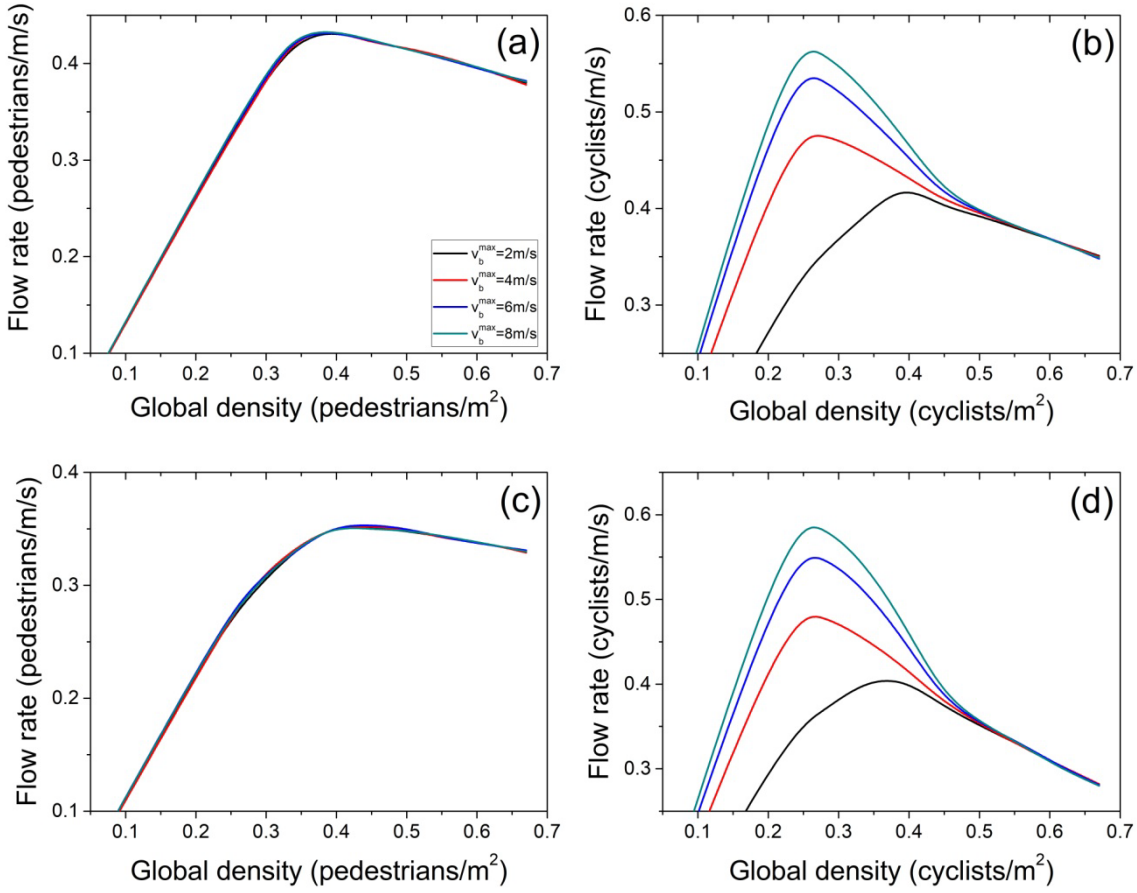

Fig. 22. Flow rate versus density at different maximum speed of cyclists on the ring-shaped track. (a) Pedestrian flow rate in unidirectional flow. (b) Cyclist flow rate in unidirectional flow. (c) Pedestrian flow rate in bidirectional flow. (d) Cyclist flow rate in bidirectional flow.

Fig. 23 shows that in both the unidirectional and bidirectional scenarios, both the pedestrian flow rate and the cyclist flow rate decreased with increasing bicycle size. This is easily understood: larger bicycles occupied more space on the track, and the space for free

movement was thus more limited when larger bicycles were present.

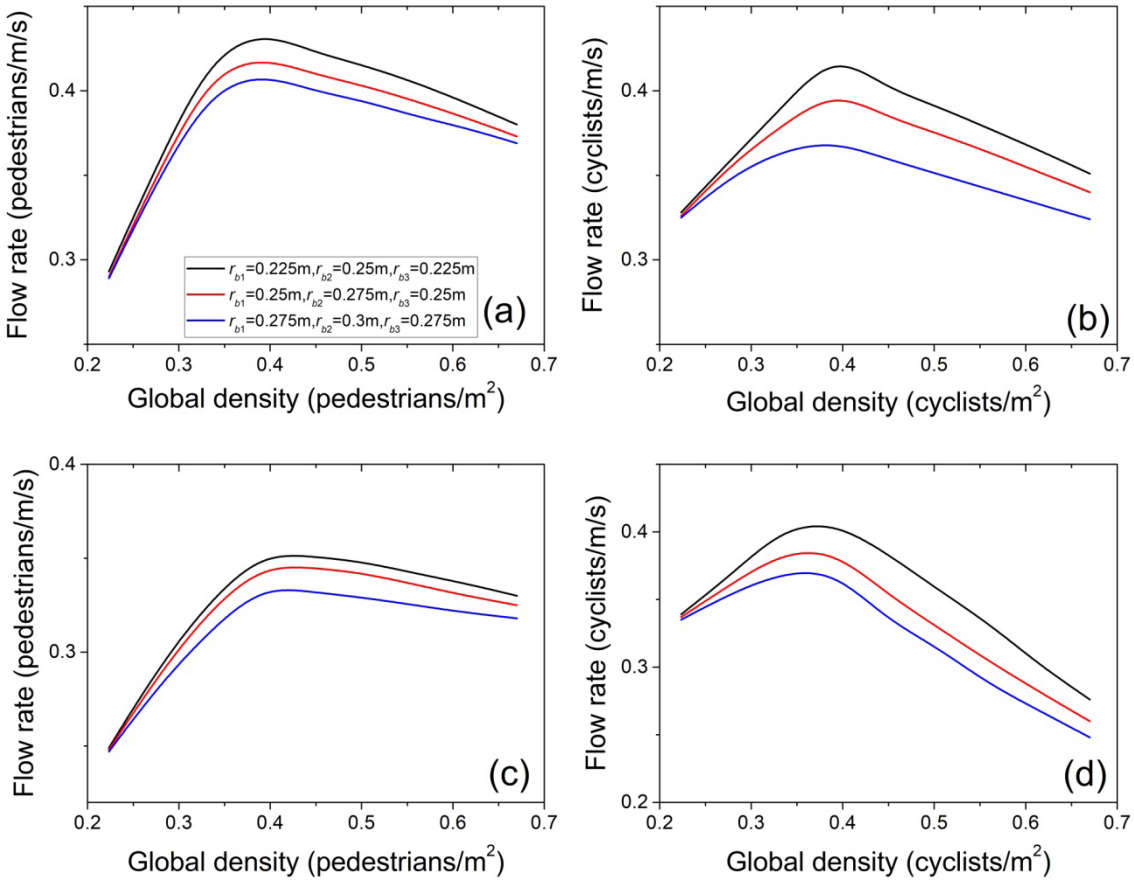

Fig. 23. Flow rate versus density at different bicycle size on the ring-shaped track. (a) Pedestrian flow rate in unidirectional flow. (b) Cyclist flow rate in unidirectional flow. (c) Pedestrian flow rate in bidirectional flow. (d) Cyclist flow rate in bidirectional flow.

Any pedestrian-cycle shared path will have different numbers of pedestrians and cyclists. Fig. 24 depicts the relationship between flow rate and density for various proportions of pedestrians and cyclists. With a fixed cyclist/pedestrian number, the maximum flow rate and the corresponding critical density of pedestrian/cyclist flow increased as the proportion of cyclists/pedestrians in both unidirectional and bidirectional flow decreased.

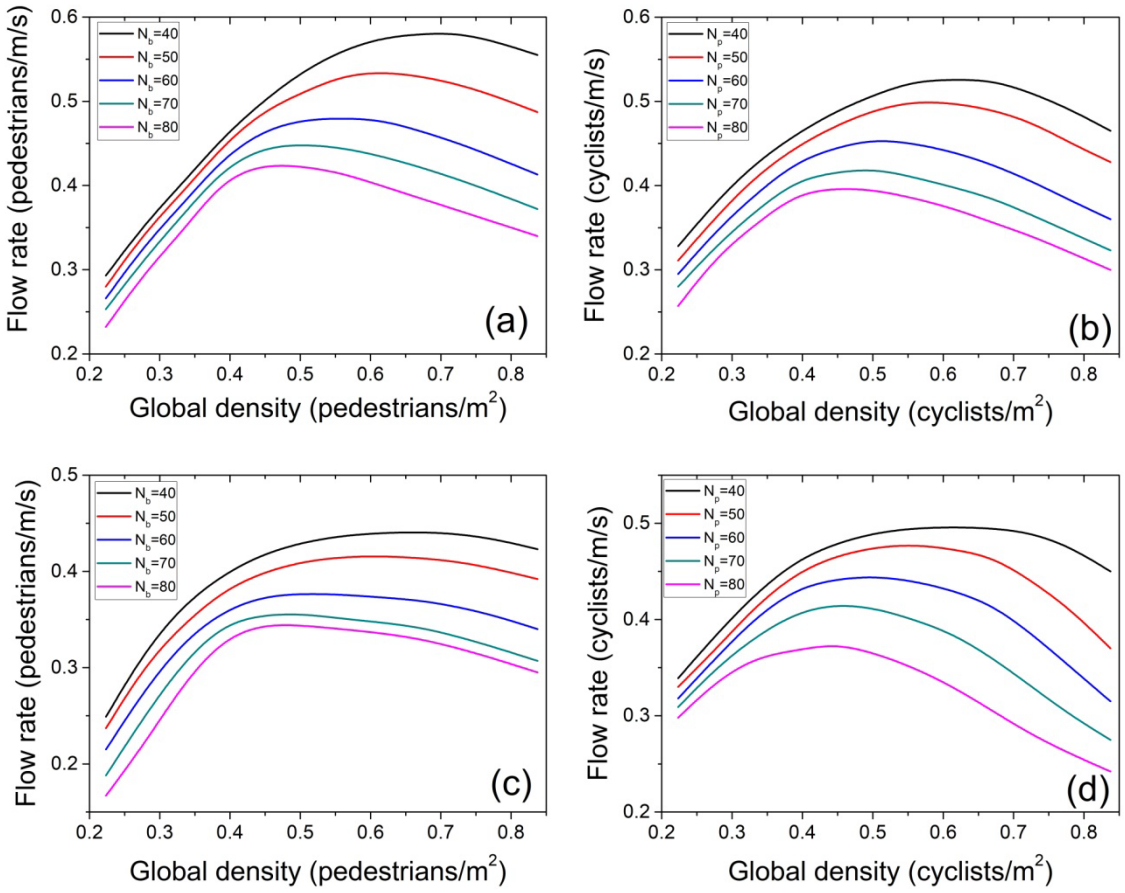

Fig. 24. Flow rate versus density at different proportions of pedestrians and cyclists on the ring-shaped track. (a) Pedestrian flow rate in unidirectional flow with fixed cyclist number. (b) Cyclist flow rate in unidirectional flow with fixed pedestrian number. (c) Pedestrian flow rate in bidirectional flow with fixed cyclist number. (d) Cyclist flow rate in bidirectional flow with fixed pedestrian number.

5.4 Simulation on the straight track

We thus further explored the flow dynamics on the straight track under the periodic boundary. The track length and width were set to 20 m and 3 m, respectively. The parameters used in the model were the same as those in Table 2 and Table 3.

Figs. 25, 26, and 27 show the snapshots of the simulations of pedestrian/cyclist distributions on the straight track. The pedestrians and cyclists could also form lanes, in both uni- and bidirectional flow. In bidirectional flow, the location distribution in the direction of the track width was more uniform. When the proportion of pedestrians was small, the pedestrians often tended to group into a few clusters, and cyclists occupied most of the track. When the proportion of pedestrians was large, cyclists moved along the track boundary to avoid the need to frequently bypass pedestrians.

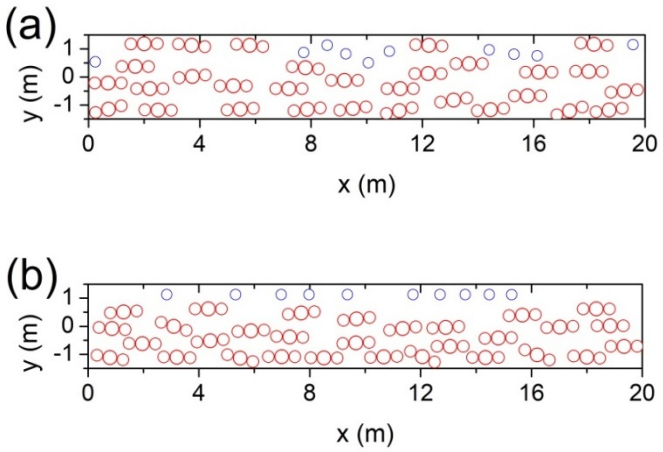

Fig. 25. Snapshots of simulations on the straight track, for 10 pedestrians + 30 cyclists. (a) Unidirectional flow. Direction of movement: left to right. (b) Bidirectional flow. Direction of movement: right to left (pedestrian), left to right (cyclist). Blue single circle: pedestrian; red three circles: cyclist.

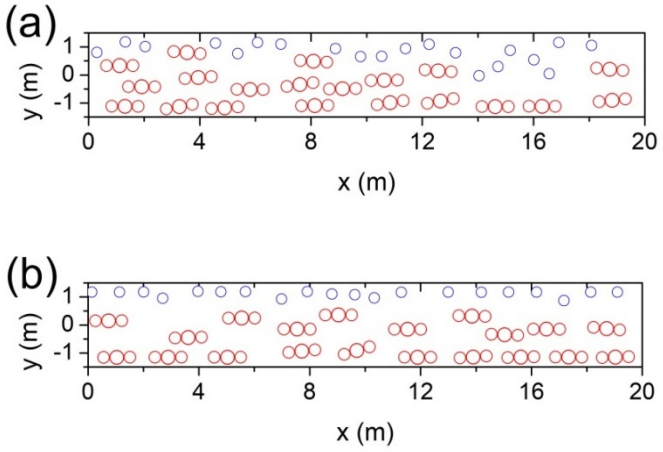

Fig. 26. Snapshots of simulations on the straight track, for 20 pedestrians + 20 cyclists. (a) Unidirectional flow. Direction of movement: left to right. (b) Bidirectional flow. Direction of movement: right to left (pedestrian), left to right cyclist). Blue single circle: pedestrian; red three circles: cyclist.

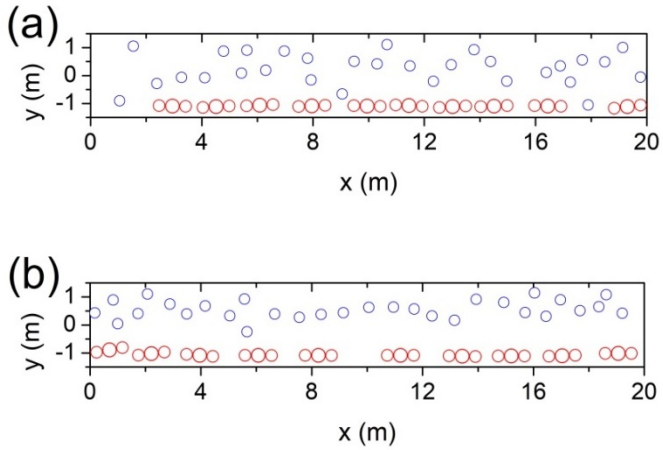

Fig. 27. Snapshots of simulations on the straight track, for 30 pedestrians + 10 cyclists. (a) Unidirectional flow. Direction of movement: left to right. (b) Bidirectional flow. Direction of movement: right to left (pedestrian), left to right (cyclist). Blue single circle: pedestrian; red three circles: cyclist.

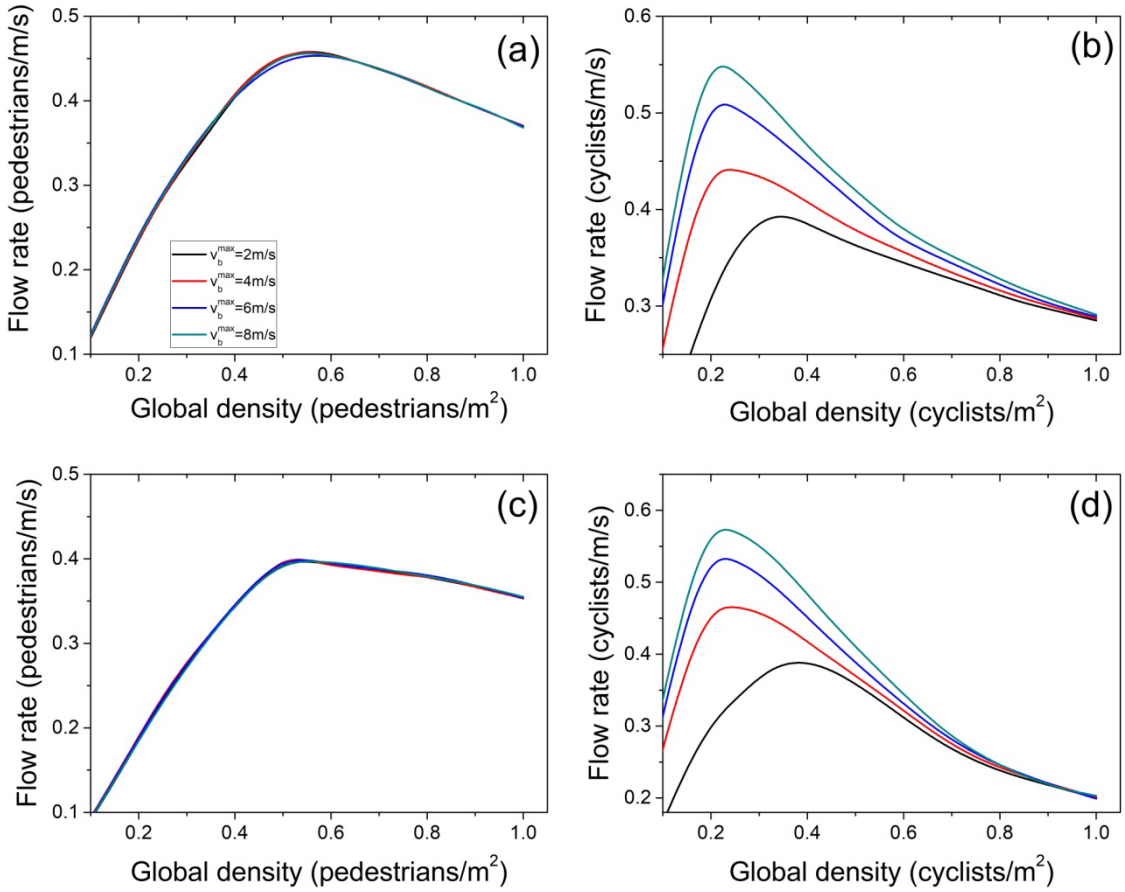

Fig. 28. Flow rate versus density at different maximum speed of bicycles on the straight track. (a) Pedestrian flow rate in unidirectional flow. (b) Cyclist flow rate in unidirectional flow. (c) Pedestrian flow rate in bidirectional flow. (d) Cyclist flow rate in bidirectional flow.

Fundamental diagrams of the straight track data, shown in Figs. 28 and 29, are largely identical to those on the ring-shaped track. As the bicycle's maximum speed increased, the relationship between the pedestrian density and the pedestrian flow rate was essentially unchanged (Fig. 28(a) and 28(c)). A higher maximum speed led to higher flow rates of cyclists in low densities. As the density increased, the difference in the cyclist flow rates decreased (Figs. 28(b) and 28(d)).

Fig. 29 depicts the trend of flow rates with different proportions of pedestrians/cyclists, and shows that larger proportions of pedestrians relative to cyclists caused the flow rate of cyclists to decrease, and vice versa. Thus, with increasing cyclist/pedestrian number, the maximum flow rate and the corresponding critical density of pedestrian/cyclist flow decreased in both the unidirectional and bidirectional scenarios.

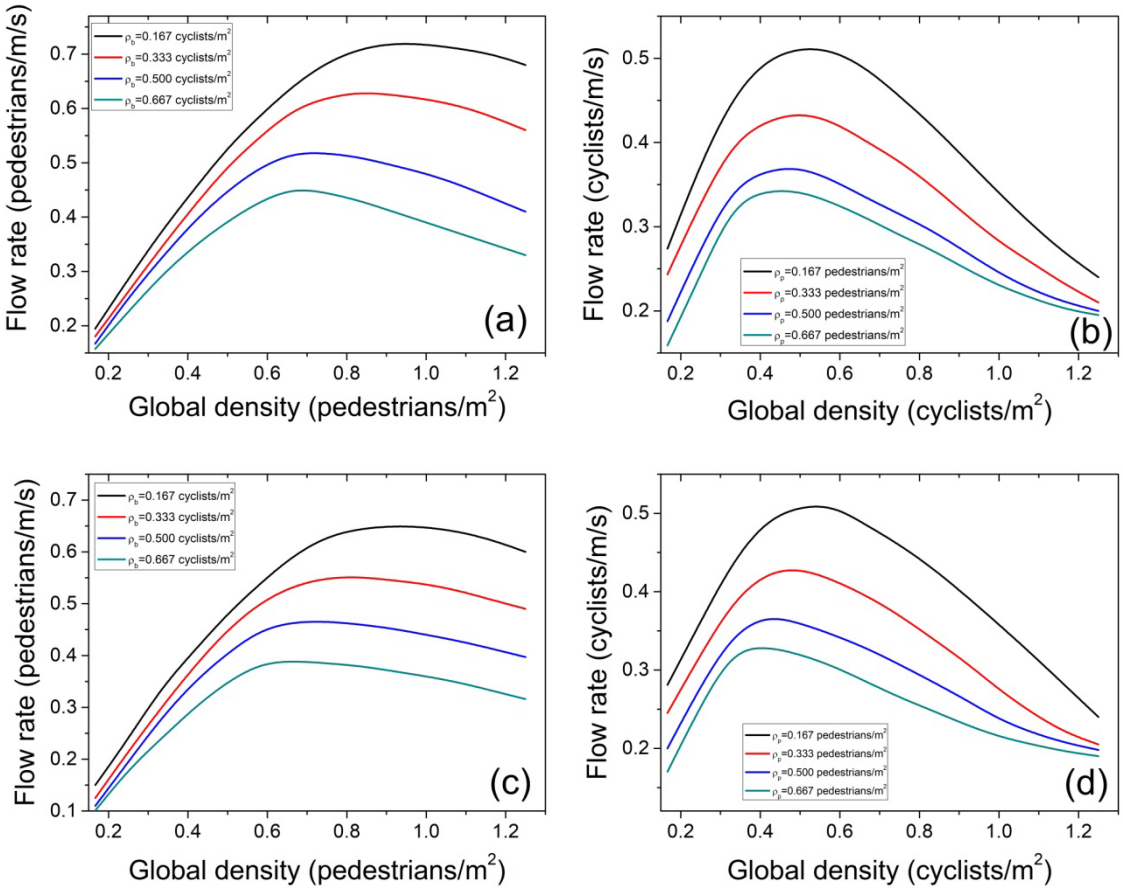

Fig. 29. Flow rate versus density at different proportions of pedestrians and cyclists on the straight track. (a) Pedestrian flow rate in unidirectional flow with fixed cyclist number. (b) Cyclist flow rate in unidirectional flow with fixed pedestrian number. (c) Pedestrian flow rate in bidirectional flow with fixed cyclist number. (d) Cyclist flow rate in bidirectional flow with fixed pedestrian number.

Fig. 30 shows a comparison of the flow rate on the ring-shaped track with that on the straight track; in both situations, the number of pedestrians was equal to the number of cyclists. One can see three key aspects, as follows. (1) For pedestrians in both unidirectional and bidirectional flow, the flow rate on the straight track is larger at a high density and smaller at a low density (Fig. 30(a) and (c)). (2) For cyclists in unidirectional flow at low density, the cyclist flow rate on the straight track is essentially the same as that on the ring-shaped track (≤0.2 cyclists/m^2), is larger at an intermediate density (0.2–0.3 cyclists/m^2), and is smaller at a high density (≥0.3 cyclists/m^2) (see Fig. 30(b)). In bidirectional flow, the situation is complicated, as seen in Fig. 30(d): the cyclist flow rate on the straight track (black line) is smaller at both low density and intermediate density, and is almost equal to that on the ring-shaped track under the same conditions, with a value of ~0.2 cyclists/m^2. However, the cyclist flow rate on the smaller ring-shaped track (blue line) is smaller/larger than that on the larger ring-shaped track (red line) at low/intermediate density. At high density, the cyclist flow rate is essentially the same on both the straight track and the ring-shaped track. (3) For pedestrians, the maximum flow rate is larger on the straight track, while for cyclists, the maximum flow rate is smaller on the straight track.

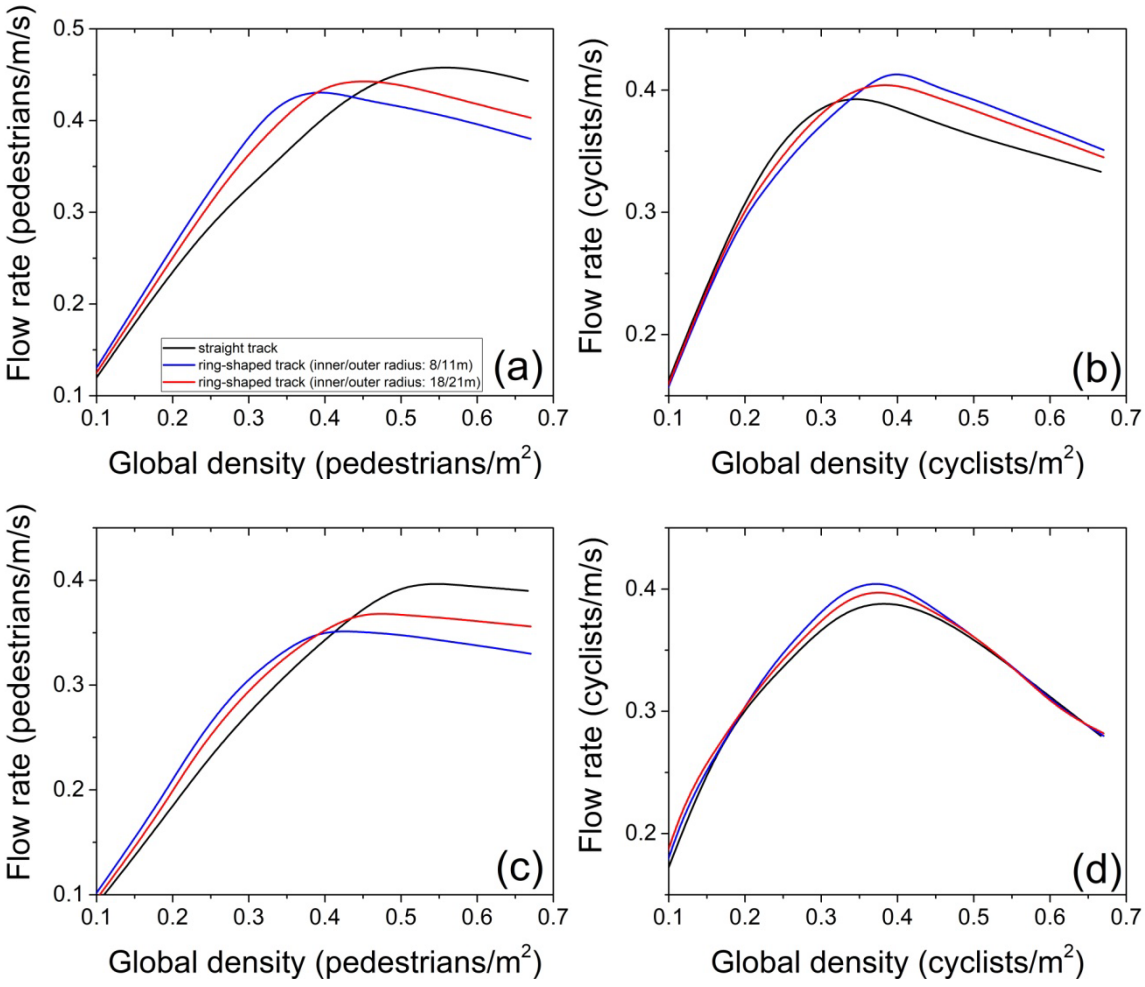

Fig. 30. Flow rate versus density on the straight track and ring-shaped track with different

inner and outer radii. (a) Pedestrian flow rate in unidirectional flow. (b) Cyclist flow rate in unidirectional flow. (c) Pedestrian flow rate in bidirectional flow. (d) Cyclist flow rate in bidirectional flow.

The results can be explained qualitatively as follows. First, let the inner radius of the ring-shaped track be r_{in}, and thus the outer radius is $r_{in} + w$. Additionally, let the effective lane-width of pedestrians be $d_{e,p}$ and that of cyclists be $d_{e,b}$. Then, in unidirectional flow, the relative difference in speed between cyclists and pedestrians was small, therefore, there was essentially no gap between the cyclist lane and the pedestrian lane, i.e., $d_{e,p} + d_{e,b} = w$. The simulations indicated that $d_{e,p}$ and $d_{e,b}$ were essentially independent of r_{in}. At a given density ρ, the number of cyclists and pedestrians $N = \rho\pi\left(\left(r_{in}+w\right)^2 - r_{in}\right)$. Therefore, the local density of pedestrians in the pedestrian lane is given by Eq. (22):

$$\rho_{ped} = \frac{N}{\pi\left(\left(r_{in}+d_{e,p}\right)^2 - r_{in}^2\right)} = \frac{\rho\left(w^2+2r_{in}w\right)}{d_{e,p}^2+2r_{in}d_{e,p}} \tag{22}$$

where the value of ρ_{ped} decreased with the increase of r_{in}. Therefore, ρ_{ped} was smaller on the straight track. At a low density ρ, a smaller ρ_{ped} led to a lower flow rate. At a large density ρ, a smaller ρ_{ped} led to a greater flow rate[2].

Similarly, the local density of cyclists in the cyclist lane is given by Eq. (23):

$$\rho_{bic} = \frac{N}{\pi\left(\left(r_{in}+w\right)^2 - \left(r_{in}+d_{e,p}\right)^2\right)} = \frac{\rho\left(w^2+2r_{in}w\right)}{w^2-d_{e,p}^2+2r_{in}\left(w-d_{e,p}\right)} \tag{23}$$

where the value of ρ_{bic} increased with the increase of r_{in}. Therefore, ρ_{bic} was greater on a straight track. At a low density ρ, a larger ρ_{bic} led to a greater flow rate; in contrast, at large density a larger ρ_{bic} led to a lower flow rate.

The simulation also indicated that $d_{e,p}$ was constant at a low density, but increased with ρ at a high density. As the maximum pedestrian flow rate was achieved at a higher density on the straight track than on the ring-shaped track, the maximum pedestrian flow rate was greater on the straight track than on the ring-shaped track.

Moreover, the interaction perimeter between pedestrians and cyclists was approximately $2\pi(r_{in} + d_{e,p})$. Therefore, the contribution of pedestrian-cyclist interactions[3] to cyclist movement was smaller on the ring-shaped track than on the straight track. Therefore, the maximum flow rate of cyclists was greater on the ring-shaped track.

---

[2] Note that this implies that the maximum pedestrian flow rate was achieved at a larger density on the straight track than on the ring-shaped track.

[3] The interaction hindered the cyclist flow but essentially did not hinder the pedestrian flow, as (i) bicycles moved faster than pedestrians, and (ii) pedestrians could not see bicycles behind them.

In bidirectional flow, the features of the pedestrian lanes were similar to those in unidirectional flow. Therefore, the result in Fig. 30(c) is similar to that in Fig. 30(a). However, as the relative speed difference between pedestrians and cyclists was much larger in bidirectional flow than in unidirectional flow, in bidirectional flow the cyclists tried to maintain a distance from the pedestrians. As a result, a gap emerged between the cyclist lane and the pedestrian lane, i.e., $d_{e,p} + d_{e,b} < w$. Consequently, the features of the cyclist lane and thus the cyclist flow in bidirectional flow were somewhat different from that in unidirectional flow, cf. Fig. 30(d) and (b).

6. Conclusions

In this study, an improved heuristic-based model was proposed for study of a mixed flow of pedestrians and cyclists. In this model, the interactions between pedestrians and cyclists in uni- and bidirectional flow were differentiated, and pedestrians/cyclists were treated as weakening the contact with individuals traveling in the opposite direction.

An experiment with a mixed flow of pedestrians and cyclists was conducted to calibrate the model. Both the simulation and experimental data showed that pedestrians and cyclists separated into two independent lanes. The widths of both the pedestrian lane and the cyclist lane were more uniform in bidirectional flow. As the density increased, the pedestrian flow rate exceeded that of the bicycles in both unidirectional and bidirectional flow scenarios. Also, the pedestrian flow rate was greater in unidirectional flow than in bidirectional flow. In contrast, at low densities the cyclist flow rate was essentially equal under the two scenarios. When the cyclist density was large, the cyclist flow rate became larger in the unidirectional flow scenario.

A comparison of the simulation and experiment results showed that our model is reliable for evaluation of the dynamics and characteristics of mixed flows of pedestrians and cyclists. Sensitivity analyses showed that at high cyclist densities, greater cyclist speeds would not effectively increase the cyclist flow rate. Moreover, the pedestrian flow rate increased as the proportion of cyclists decreased, and vice versa. The simulation results on the straight track were similar to those on the ring-shaped track.

The model can be used to evaluate the capacity and level-of-service of pedestrian-cycle shared-use roads. In reality, this model can be calibrated with empirical data on pedestrian-cyclist mixed flow. There are two types of empirical data that can be considered (see Wolinski et al., 2014): microscopic data (trajectory data on pedestrians and cyclists in mixed flow conditions), and macroscopic data (the aggregate characteristics of the pedestrian and bicycle flows). The calibration process involves two procedures to determine the

calibrated parameters (see Hussein and Sayed., 2018). The first is direct calibration, i.e., calibration of parameters that can be observed directly such as the desired speed, which can be obtained by measuring the speed in the free-flow state when individuals have no interaction with others. The second is indirect calibration, i.e., calibration of parameters that cannot be measured directly. Empirical data on pedestrian-cyclist mixed flow can be obtained in the real world by filming a section of a pedestrian-bicycle-shared road and then extracting the trajectory of each pedestrian and cyclist. In our model, $v_{\max}$ can be directly calibrated when the density is very low and pedestrians and cyclists have no interaction with others. Other parameters, including τ_1, τ_2, τ_3, τ_4, and T_{safe}, need to be calibrated indirectly, e.g., using the empirical relationship between density and flow rate, which can be measured as shown in Section 5.2.

In future work, we will conduct experiments to validate our model using more participants and different proportions of pedestrians/cyclists. An experiment to change directions of cyclists in unidirectional and bidirectional flow will also be carried out to examine the effect of right/left turning of cyclists on the dynamics of pedestrian-cyclist mixed flow.

Acknowledgments

This work was supported by the National Key R&D Program of China (No. 2018YFB1600900), National Natural Science Foundation of China (Grants No. 71931002, 71801066, 71621001), the Research Grants Council of the Hong Kong Special Administrative Region, China (Project No. 17201318), and the Fundamental Research Funds for the Central Universities (Grant No. JZ2020HGTB0021, 2016RC009).

References

Bassett Jr, David R, Pucher J, Buehler, R, Thompson L, Crouter S (2008) Walking, cycling, and obesity rates in Europe, North America, and Australia. J. Phys. Act. Health 5: 795-814.

Bernardi S, Rupi F (2015) An analysis of bicycle travel speed and disturbances on off-street and on-street facilities. Transp. Res. Proc. 5: 82-94.

Burstedde C, Klauck K, Schadschneider A, Zittartz J (2001) Simulation of pedestrian dynamics using a two-dimensional cellular automaton. Physica A 295: 507-525.

Chattaraj U, Seyfried A, Chakroborty P (2009) Comparison of pedestrian fundamental diagram across cultures. Adv. Complex Syst. 12: 393-405.

Chen J, Xie Z Q (2009) Cycle traffic conflict model on urban pedestrian-bicycle paths J. Jilin Univ. 39: 121-125. (in Chinese)

Davidich M, Köster G (2012) Towards automatic and robust adjustment of human behavioral parameters in a pedestrian stream model to measured data. Safety Sci. 50, 1253-1260.

Deng J (2011) Mixed traffic flow cellular automaton model based on shared-use sidewalk. J. Transp. Syst.

Eng. Inf. Technol. 11: 155-159. (in Chinese)
Flötteröd G, Lämmel G (2015) Bidirectional pedestrian fundamental diagram. Transp. Res. Part B 71: 194-212.
Guo N, Jiang R, Wong S C, Hao Q Y, Xue S Q, Hu M B (2019) Bicycle flow dynamics on wide roads: experiment and modeling. ArXiv: 1904.06084.
He X Q, Lin B Q (2000) Safety engineering. China University of Mining and Technology Press, Xuzhou, 43-47.
Helbing D, Molnár P (1995) Social force model for pedestrian dynamics. Phys. Rev. E 51: 4282-4286.
Helbing D, Farkas I, Vicsek T (2000) Simulating dynamical features of escape panic. Nature 407: 487-490.
Helbing D, Farkas I J, Molnár P, Vicsek T (2002) Simulation of pedestrian crowds in normal and evacuation situations. Pedestrian Evacuation Dynamics (Springer) eds. Schreckenberg, M. and Sharma, S. D. 21-58.
Helbing D, Buzna L, Johansson A, Werner T (2005) Self-organized pedestrian crowd dynamics: experiments, simulations, and design solutions. Transport. Sci. 39: 1-24.
Hughes R L (2002) A continuum theory for the flow of pedestrians. Transp. Res. B - Meth 36: 507-535.
Hussein M, Sayed T (2018) Validation of an agent-based microscopic pedestrian simulation model at the pedestrian walkway of Brooklyn Bridge. Transport. Res. Rec. 2672: 33-45.
Jiang R, Jia B, Wu Q S (2004) Stochastic multi-value cellular automata models for bicycle flow. J. Phys. A 37:2063-2072.
Jia B, Li X G, Jiang R, Gao Z Y (2007) Multi-value cellular automata model for mixed bicycle flow. Eur. Phys. J. B 56:247-252.
Jiang R, Hu M B, Wu Q S, Song W G (2017) Traffic dynamics of bicycle flow: experiment and modeling. Transport. Sci. 51: 998-1008.
Kang L, Xiong Y, Mannering F (2013) Statistical analysis of pedestrian perceptions of sidewalk level of service in the presence of bicycles. Transport. Res. A 53: 10-21.
Kwon Y, Morich S, Yai T (1997) Analysis of behaviors and interactions of pedestrians, bicycles and cars in narrow urban streets. J. East. Asia Soc. Transp. Stud. 2: 853-862.
Lam W, Lee J, Chan K, Goh P (2003) A generalised function for modeling bidirectional flow effects on indoor walkways in Hong Kong. Transp. Res. Part A Policy Pract. 37: 789-810.
Li Z B, Ye M, Li Z, Du M Q (2015) Some operational features in bicycle traffic flow observational study. Transport. Res. Rec. 2520:18-24
Liang X, Mao B, Xu Q (2012) Psychological-physical force model for bicycle dynamics. J. Transport. Sys. Eng. Inform. Technol., 2012, 12, 91-97.
Liu Z X, Wang X Y, Wang J Q, Wang F, Liu Y Q, Wang J H (2018) Pedestrian movement intention identification model in mixed pedestrian-bicycle sections based on phase-field coupling theory. Adv. Mech. Eng. 10: 1-14.
Mao Y T (2015) Research of mixed slow traffic flow simulations based on cellular automata model. Suzhou University of Science and Technology. (Master thesis in Chinese)
Ministry of Housing and Urban-Rural Development, State Development and Reform Commission, Ministry of Finance (2012) Guidelines on strengthening urban pedestrian and bicycle transport systems. Urban Development Document 133: 1-8.
Moussaïd M, Helbing D, Theraulaz G (2011) How simple rules determine pedestrian behavior and crowd disasters. Proc. Nat. Acad. Sci. USA 108: 6884-6888.
Moussaïd M, Guillot E G, Moreau M, Fehrenbach J, Chabiron O, Lemercier S, Pettre J, Appert-Rolland C,

Degond P, Theraulaz G (2012) Traffic instabilities in self-organized pedestrian crowds. PLoS Comput. Biol. 8: e1002442.
Muramatsu M, Irie T, Nagatani T (1999) Jamming transition in pedestrian counter flow. Physica A 267: 487-498.
Navin F P D, Wheeler R J (1969) Pedestrian flow characteristics. Traffic Eng. Control 39: 31-36.
Navin F P D (1994) Bicycle traffic flow characteristics: experimental results and comparisons. ITE J. 64:31-36.
Tadaki S, Kikuchi M, Fukui M, Nakayama A, Nishinari K, Shibata A, Sugiyama Y, Yosida T, Yukawa S (2013) Phase transition in traffic jam experiment on a circuit. New J. Phys. 15: 103034.
Tang T Q, Huang H J, Shang H Y (2010) A dynamic model for the heterogeneous traffic flow consisting of car, bicycle and pedestrian. Int. J. Mod. Phys. C 21: 159-176
Wierbos MJ, Knoop VL, Hänseler FS, Hoogendoorn SP (2019) Capacity, capacity drop, and relation of capacity to the path width in bicycle traffic. Transport. Res. Rec. DOI: 10.1177/0361198119840347
Wolinski D, Guy S J, Olivier A H, Lin M, Manocha D, Pettré J (2014) Optimization-based pedestrian model calibration for evaluation. Transport. Res. Pro. 2: 228-236.
Xie Z Q (2009) link operational characteristics and resources optimization allocation of bicycle-pedestrian shared-use paths. Nanjing: Southeast University. (Dissertation in Chinese)
Xue S Q, Jia B, Jiang R, Li X G, Shan J J (2017) An improved Burgers cellular automaton model for bicycle flow. Physica A 487:164-177.
Yu H, Chen J, Xie Z Q (2012) Level of service model on urban cycle-pedestrian roads. Urban Transport of China 10: 75-79. (in Chinese)
Zacharias J (1999) The Amsterdam experiment in mixing pedestrians, trams and bicycles. ITE J. 8: 22-28.
Zhang J, Klingsch W, Schadschneider A, Seyfried A (2011) Transitions in pedestrian fundamental diagrams of straight corridors and T-junctions. J. Stat. Mech: Theory Exp. P06004.
Zhang J, Klingsch W, Schadschneider A, Seyfried A (2012) Ordering in bidirectional pedestrian flows and its influence on the fundamental diagram. J. Stat. Mech: Theory Exp. P02002
Zhang J, Mehner W, Holl S, Boltes M, Andresen E, Schadschneider A, Seyfried A (2014) Universal flow-density relation of single-file bicycle, pedestrian and car motion. Phys. Lett. A 378: 3274-3277.
Zhao Y X, Zhang H M (2017) A unified follow-the-leader model for vehicle, bicycle and pedestrian traffic. Transp. Res. B - Meth 105: 315-327.

Appendix

We examine the assumption (iii) in our model concerning evaluation of collision distance. In our model, the cyclists assume that other cyclists and pedestrians traveling in the same direction do not move. This is due to the fact that bicycles require a short stopping distance, particularly when a road is congested. In contrast, if each cyclist assumes that pedestrians and cyclists in the same direction move with current speed, the cyclists can follow the cyclists/pedestrians in front of them at a high speed even in high-density conditions, leading to overly high flow rates in medium/high density conditions (see Fig. A1).

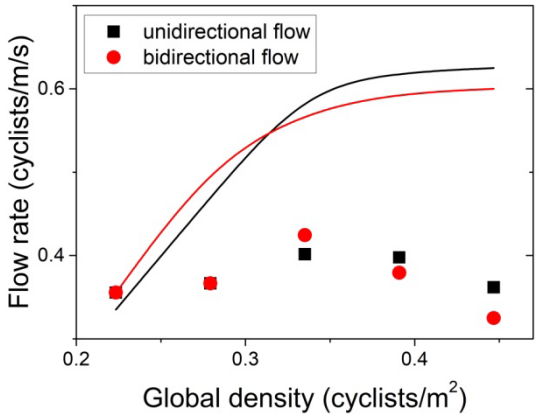

Fig. A1. Fundamental diagram. In the simulation, each cyclist assumes that pedestrians and cyclists in the same direction move with current speed.